Mechanisms of antiproton annihilation and dynamics of baryon exchange

B. G. Zakharov
Institute of Nuclear Physics, Moscow State University

B. Z. Kopeliovich
Joint Institute for Nuclear Research, Dubna

Fiz. Elem. Chastits At. Yadra **22**, 140–203 (January–February 1991)

A succession of antiproton-annihilation mechanisms corresponding to variation of the energy from superhigh to low values (hundreds of mega-electron-volts) is considered. It is shown in QCD perturbation theory that annihilation in the asymptotic region is associated with color decuplet gluonic exchange leading to the production of three-string configurations. The cross section of this process does not depend on the energy and is $(1–2) \times 10^{-27}$ cm^2. Data analysis has confirmed the presence of such a contribution with cross section $(1.5 \pm 0.1) \times 10^{-27}$ cm^2. In the intermediate range of energies (tens of giga-electron-volts) the dominant processes in the annihilation are associated with the retardation of one of the valence quarks and transition of the diquark from the triplet to the sextet color state. It is shown that at low energies the cross section of the pp interaction increases so strongly that the unitarity corrections give rise to an anomalous growth of the interaction range.

INTRODUCTION

One of the processes associated with baryon-number transfer is baryon annihilation, i.e., an interaction of a baryon and an antibaryon in which only mesons are produced in the final state. Since these interaction channels are absent in baryon collisions, the question arises of the manner in which baryon annihilation is connected by the unitarity relation to the elastic scattering amplitude, and whether the annihilation corresponds to C-even or C-odd exchanges in the crossed channel. Another related question is that of why the cross section of $\bar{p}p$ annihilation measured at energies $E \leqslant 12$ GeV is close to the difference of the total $\bar{p}p$ and pp interaction cross sections. This experimental observation led to popularity of the naïve point of view according to which the annihilation is related by unitarity to the ω Reggeon responsible in Regge phenomenology for the difference between the $\bar{p}p$ and pp interaction cross sections. This, at the first glance natural, interpretation encounters serious difficulties in a deeper study of the process. The ω-Reggeon exchange has quark structure $\bar{q}q$. Cutting of the ω Reggeon, i.e., study of the inelastic processes associated with it by unitarity, reveals the presence of nonannihilation channels. In addition, there exist processes, for example, the $\Delta^{++}\bar{\Delta}^{-}$ interaction, in which baryon exchange, i.e., annihilation, is possible. At the same time, a contribution of ω exchange in the elastic channel is impossible because of the difference between the quark contents of the colliding baryons.

Identification of the difference between the total $\bar{p}p$ and pp interaction cross sections with annihilation leads to a further paradox. It is known that the difference of the partial amplitudes of elastic $\bar{p}p$ and pp scattering has a peripheral nature. This is directly seen, for example, from the fact that the corresponding difference of the differential cross sections changes sign at $|t| \approx 0.2$ GeV^2 ("crossover" effect). On the other hand, the hadrons produced in $\bar{p}p$ annihilation have an enhanced transverse momentum, indicating a central nature of the annihilation.

Thus, the assumption of an unambiguous connection between the annihilation and the ω Reggeon does not stand up to criticism, and the observed equality of the difference between the total cross sections and the annihilation cross section is apparently fortuitous (although, as will be shown below, the energy dependence must be the same).

Of course, one could attempt to adopt a different point of view and assume that the traditional Regge phenomenology incorrectly ascribes the difference between the total $\bar{p}p$ and pp interaction cross sections to the contribution of ω exchange. However, as will be shown below, this possibility also leads to serious contradictions.

Naturally, all these problems can be solved only in the framework of a definite dynamical approach to the description of soft hadron collisions at high energies. Unfortunately, the construction of such an approach on the basis of QCD first principles is as yet impossible. Nevertheless, the ideas of QCD are very fruitful for the development of model approaches. At the present time, the most successful popular model of soft hadron interactions at high energies is the model of quark–gluon strings (MQGS).[1–8] This model is based on the topological-expansion scheme[9,10] and the representation of the hadron-production mechanism in the form of breaking of the color tubes (strings) into sections formed as a consequence of confinement in the vacuum when color exchanges take place between the initial particles.[11–13] For processes without the participation of baryons, the leading terms of the topological expansion are equivalent to the terms of leading order in the expansion in $1/N$ ($N = N_c$, $N_c/N_F = \text{const}$) in QCD.[14] In the topological-expansion scheme, exchanges of secondary Reggeons are described by planar diagrams, and Pomeron exchange by a cylindrical diagram. When the idea of confinement is added to the topological-expansion scheme in the MQGS, the hadron states associated with the cut of each sheet of a

topological diagram are represented in the form of the decay products of one triplet string. At the same time, for the interaction of mesons the cut of the planar Reggeon diagram of the topological expansion corresponds to the formation, on the annihilation of a $\bar{q}q$ pair from the initial particles, of a triplet string with a quark and an antiquark at its ends. The cut of the cylindrical diagram of the topological expansion corresponds to the production of two $\bar{q}q$ strings.

The fact that the number of quarks in the baryon is equal to the number of colors means that it is not possible to justify the topological expansion of the amplitudes of processes with the participation of baryons on the basis of the $1/N$ expansion in QCD.[15–17] When these processes are analyzed in practice in the MQGS, the pair of quarks in the baryon (called the diquark D) in the $\{\bar{3}\}$ color state is treated like the antiquark in a meson. In this case, reactions with the participation of baryons are analyzed in the same way as the interaction of mesons. However, this device is in no way justified, since one can see no particular reasons why transitions of diquarks to sextet color states should be suppressed in the collision process. The unsatisfactory nature of this approach is especially clearly manifested in its inability to describe the experimental data on $\bar{p}p$ annihilation. Indeed, in this treatment of the MQGS (below, we shall call it the standard one), the intermediate states corresponding to the cut of the Pomeron and the secondary Reggeon contain a $D_{\{\bar{3}\}}\bar{D}_{\{3\}}$ string, which on the breaking as a result of production of $\bar{q}q$ pairs leads to the production of a baryon and an antibaryon in the region of fragmentation of the initial baryon and antibaryon. The meson channels can be coupled only to a cut of the diagram with $\bar{D}D$-Reggeon exchange, which in the intermediate state corresponds to a $\bar{q}q$ string. The cross section of $\bar{B}B$ annihilation for this mechanism decreases with the energy as $s^{\alpha_{\bar{D}D}(0)-1}$, where $\alpha_{\bar{D}D}(0)$ is the intercept of the $\bar{D}D$ trajectory (we ignore the possibility of production of $\bar{B}B$ pairs in the triplet string). It is possible to estimate $\alpha_{\bar{D}D}(0)$, either from Kaĭdalov's s-channel factorization relations,[18] which relate $\alpha_{\bar{D}D}(0)$ to the intercepts of the baryon and meson trajectories $\{2\alpha_B(0) = \alpha_{\bar{D}D}(0) + \alpha_{q\bar{q}}(0)]$, or from fits to the distribution function of the diquarks in the baryon, which depends on $\alpha_{\bar{D}D}(0)$, in the framework of the MQGS. Both methods give a low value for the intercept of the $\bar{D}D$ trajectory: $\alpha_{\bar{D}D}(0) \lesssim -0.5$. Thus, the annihilation cross section associated with $\bar{D}D$ annihilation decreases rapidly with the energy as $\sim s^{-1.5}$. Therefore, this mechanism cannot explain the dependence $\sigma^{\bar{p}p}_{\text{ann}} \propto s^{-1/2}$ observed at energies near 10 GeV.

Because the experimentally observed behavior of $\sigma^{\bar{p}p}_{\text{ann}}$ cannot be due to production of a $\bar{q}q$ string on the annihilation of diquarks, the following question arises: What string configurations are responsible for $\bar{p}p$ annihilation? Such a formulation of the problem appears sensible if one does not reject the assumption, based on the confinement idea, that in $\bar{p}p$ annihilation the mesons are produced as a result of breaks in the section of the tubes of the chromoelectric field. Of course, it is important to establish the t-channel exchanges to which the annihilation channels

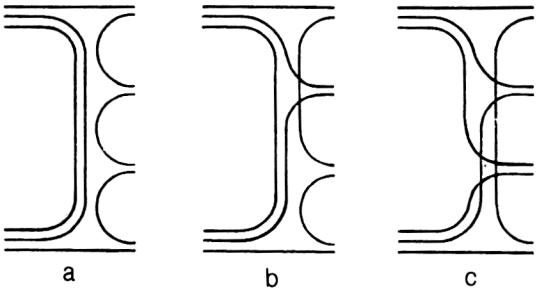

FIG. 1. Examples of quark diagrams for baryon annihilation in the approach of Eylon and Harari.[23]

are related by the unitarity condition. In the literature, there are various approaches to these two questions.

Recently, the most popular point of view (Refs. 1, 5, 6, 15, 16, and 19–22) has been that the dependence $\sigma^{\bar{p}p}_{\text{ann}} \propto s^{-1/2}$ observed at $E_{\text{lab}} \sim 10$ GeV is due to the formation of three $\bar{q}q$ strings. The acceptance of this point of view was helped by the results of a paper of Eylon and Harari,[23] which was completed before the appearance of the MQGS. In Ref. 23, baryon annihilation was described by quark diagrams with emission of mesons by one, two, or three quark lines (Fig. 1). It was also assumed that the emission of mesons by the quarks for diagrams like those of Fig. 1 proceeds in the same way as in the case of the Reggeon with $\bar{q}q$ structure. The contributions of diagrams like those of Fig. 1 to the annihilation cross section were calculated in the Chew–Pignotti multiperipheral approach. The following estimates were obtained for the intercepts that determine the energy dependence of the contribution of the mechanisms of Fig. 1 to the $\bar{B}B$ annihilation cross section:

$$\alpha^{(a)}(0) = 2\alpha_B(0) - \alpha_R(0); \tag{1}$$

$$\alpha^{(b)}(0) = 2\alpha_B(0) + 1 - 2\alpha_R(0); \tag{2}$$

$$\alpha^{(c)}(0) = 2\alpha_B(0) + 2 - 3\alpha_R(0). \tag{3}$$

Here, $\alpha_B(0)$ is the intercept of the baryon trajectory, and $\alpha_R(0)$ is the intercept of the secondary Reggeon trajectory. Setting $\alpha_B(0) = 0$ and $\alpha_R(0) = 0.5$, Eylon and Harari[23] obtained $\alpha^{(a)}(0) = -0.5$, $\alpha^{(b)}(0) = 0$, $\alpha^{(c)}(0) = 0.5$. Thus, the energy dependence of the contribution of diagrams like those of Fig. 1c to the annihilation cross section (the dominant contribution in the asymptotic region) agreed with the experimentally observed dependence of $\sigma^{\bar{p}p}_{\text{ann}}$ at $E_{\text{lab}} \sim 10$ GeV. Of course, the possibility of using the multiperipheral model in baryon exchanges is questionable. We shall show below that the numerical estimates obtained in Ref. 23 for the two contributions to the annihilation cross section that decrease most slowly with the energy are incorrect.

Eylon and Harari[23] also argued that the annihilation channels correspond in the sense of the unitarity condition to Pomeron exchange. Considering the contributions of the processes $BB \to BB + nM$ and $\bar{B}B \to \bar{B}B + nM$ (M is a meson) to the unitarity relation, they found that the number of quark diagrams with vacuum quantum numbers in the t

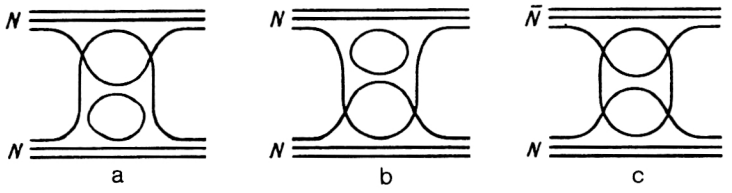

FIG. 2. Quark diagrams for amplitudes of NN scattering (a, b) and $\bar{N}N$ scattering (c), related by the unitarity condition to the processes $NN \to NN + nM$ and $\bar{N}N \to \bar{N}N + nM$ for $n = 1$.

channel for BB scattering was equal to 2^n, and for $\bar{B}B$ scattering to $2^n - 1$. The corresponding example for $n = 1$ is shown in Fig. 2. For $\alpha_R(0) = 0.5$, this difference between the numbers of diagrams leads to a difference between the BB and $\bar{B}B$ cross sections that decreases as $s^{-1/2}$. Eylon and Harari suggested that the missing contribution to the $\bar{B}B$ interaction cross section should be identified with the contribution of the annihilation channels. As they themselves recognized,[23] their argument that the annihilation channels can be included in the cutting of the Pomeron is qualitative in nature. Another shortcoming of the argument is that the possibility of compensating the difference between the cross sections of the processes $BB \to BB + nM$ and $\bar{B}B \to \bar{B}B + nM$ by the contribution of the annihilation channels in the framework of the multiperipheral model appears fortuitous. In the framework of this model the difference between the cross sections of the nonannihilation processes to BB and $\bar{B}B$ collisions does not depend on $\alpha_B(0)$, whereas the behavior of the $\bar{B}B$ annihilation cross section is essentially related to $\alpha_B(0)$. It is also unclear why the compensation mechanism proposed in Ref. 23 must work for $t \neq 0$, since the t dependence of diagrams like those of Fig. 2 and of multiperipheral diagrams with baryon exchanges can be different.

In Refs. 15 and 16, Rossi and Veneziano proposed a generalization of the topological-expansion scheme to the case of processes with the participation of baryons. In their approach, $\bar{B}B$ annihilation is described by diagrams with exchange of a string junction (Fig. 3). In the scheme of the topological expansion developed in Refs. 15 and 16, the trajectory of the string junction is the intersection of three sheets. The concept of the string junction arises naturally in the string model of a baryon with a Y configuration,[24] and also from the gauge-invariant expression of the operator with quantum numbers of the baryon:[15,16]

$$B_{\alpha\beta\gamma} = \varepsilon^{i_1 i_2 i_3} \left[P \exp\left(ig \int_{p(x,x_1)} A_\mu dx^\mu \right) q_\alpha(x_1) \right]_{i_1} \times \left[P \exp\left(ig \int_{p(x,x_2)} A_\mu dx^\mu \right) q_\beta(x_2) \right]_{i_2} \times \left[P \exp\left(ig \int_{p(x,x_3)} A_\mu dx^\mu \right) q_\gamma(x_3) \right]_{i_3}.$$

Here, A_μ and q_α are the operators of the gluon and quark fields; $p(x,x_i)$ is the path of the integration from the point x_i to the coordinate of the string junction.

The annihilation mechanisms of Fig. 3 are related to the cuts between the lines of the string junctions in the diagrams of Fig. 4, which correspond to exchanges of new Reggeons M_4^J, M_2^J, and M_0^J (we use the notation of Rossi and Veneziano[16]). The string configurations of the hadrons that must lie on the trajectories of M_4^J, M_2^J, and M_0^J are given in the upper part of Fig. 4.

Unfortunately, the method of topological classification of the annihilation mechanisms is not supported by any scheme for calculating the cross sections. Rossi and Veneziano took the values of the intercepts of the Regge trajectories M_4^J, M_2^J, and M_0^J to be -0.5, 0, and 0.5, using estimates made in the paper of Eylon and Harari[23] [see Eqs. (1)–(3)], Thus, like them, Rossi and Veneziano attributed the dependence $\sigma_{\text{ann}}^{\bar{p}p} \propto s^{-1/2}$ observed at $E_{\text{lab}} \sim 10$ GeV to three-sheet events. However, it is important that, in contrast to Eylon and Harari,[23] Rossi and Veneziano[15,16] assumed that the three-sheet events were associated, not with the Pomeron cut, but with the cut of the Reggeon M_0^J.

In the topological approach of Rossi and Veneziano, some difficulties arise if the dependence $\sigma_{\text{ann}}^{\bar{p}p} \propto s^{-1/2}$ is attributed to the diagram of Fig. 3c. The first problem is due to the fact that in the approach of Refs. 15 and 16 the properties of the ordinary $\bar{q}q$ Reggeons must differ appreciably from those predicted in the planar Reggeon model. Indeed, according to Refs. 15 and 16 the cross-section difference $\Delta\sigma_{\text{tot}}^{pp} = \sigma_{\text{tot}}^{\bar{p}p} - \sigma_{\text{tot}}^{pp}$ can be expressed as

$$\Delta\sigma_{\text{tot}}^{pp} \simeq 2\sigma_\omega + \sigma_J, \tag{4}$$

where σ_ω and σ_J are the contributions to $\Delta\sigma_{\text{tot}}^{pp}$ of ω and all the $M_{4,2,0}^J$ Reggeons, respectively. Making the choice $\alpha_{M_0^J}(0) = 0.5$, one can identify σ_J with $\sigma_{\text{ann}}^{\bar{p}p}$, since the term dominant in σ_J, $\sigma_{M_0^J}$, is associated solely with annihilation events. Then the experimentally observed relation $\Delta\sigma_{\text{tot}}^{pp} \approx \sigma_{\text{ann}}^{\bar{p}p}$ means that there is strong suppression of the

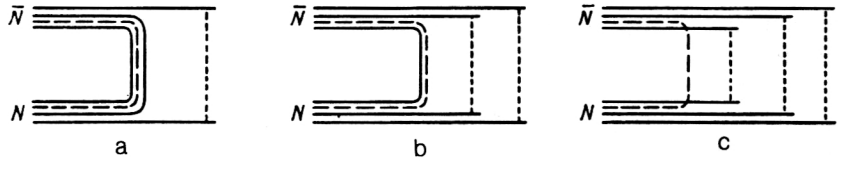

FIG. 3. Mechanisms of $\bar{B}B$ annihilation in the approach of Rossi and Veneziano[15,16] associated with exchange of a string junction (broken line).

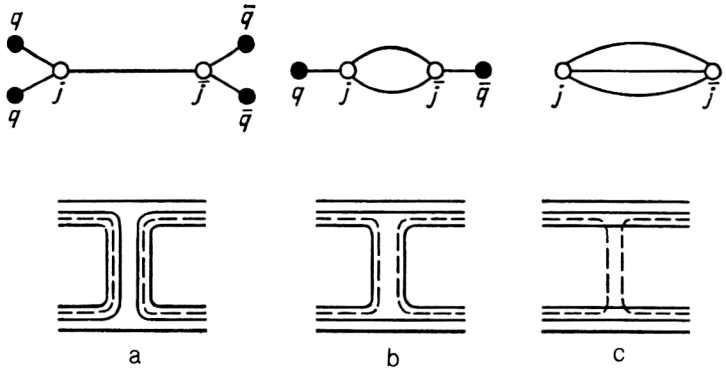

FIG. 4. Contributions to the $\bar{B}B$ scattering amplitude from exchanges of M_4^J, M_2^J, M_0^J Reggeons, related by the unitarity condition to the annihilation mechanisms of Figs. 3a–3c.

contribution of the ω Reggeon: $2\sigma_\omega \ll \Delta\sigma_{\text{tot}}^{pp}$. On the other hand, the planar Reggeon model predicts the relation $\sigma_\omega = 9\sigma_\rho$, which leads to the estimate $2\sigma_\omega \approx (0.6\text{–}0.8)\Delta\sigma_{\text{tot}}^{pp}$. To obtain this estimate, σ_ρ can be determined either from the data on the total cross sections[25] or from the factorization relation $\sigma_\rho^{NN} = (\sigma_\rho^{\pi N})^2/\sigma_p^{\pi\pi}$, where $\sigma_\rho^{\pi\pi}$ can be found from analysis of data on inelastic πN interactions.[26] Thus, the planar structure of the $\bar{q}q$ Reggeons assumed in the topological-expansion scheme is incompatible with the annihilation model proposed in Refs. 15 and 16 for the choice $\alpha_{M_0^J}(0) = 0.5$.

The suppression $\sigma_\omega \ll \sigma_J$ that follows from (4) also contradicts the widely accepted explanation of the experimentally observed growth with the energy of the inclusive spectra in pp interactions in the central range of rapidities. In the MQGS,[3] this phenomenon is related to transfer of a quark to the central region of rapidities, i.e., it is related to the contribution of a cylindrical Pomeron graph with one undeveloped sheet. If one does not introduce the unnatural assumption that the $\overline{\text{SJ}}$–SJ pair (SJ: string junction) annihilates with much greater probability than a $\bar{q}q$ pair, the inequality $\sigma_\omega \ll \sigma_J$ means that a string junction is transferred to the central region of rapidities much more often than a valence quark. But then there is formed in the central region of rapidities a three-string configuration with enhanced particle density, and this leads, not to growth, but to a decrease with the energy of the inclusive spectra. Note that the possibility of transfer of a string junction through a large rapidity interval was considered in Ref. 22 in connection with the question of the Eylon–Harari compensation mechanism. However, this difficulty in the explanation of the energy growth of the inclusive spectra was not noted.

In the model of Rossi and Veneziano,[15,16] a further difficulty arises from the values of the intercepts of the new Reggeons that they chose. For if $\alpha_{M_0^J}(0) = 0.5$, then it follows from the condition $\Delta\sigma_{\text{tot}}^{\bar{p}p} \approx \sigma_{\text{ann}}^{\bar{p}p}$ that the difference between the amplitudes of elastic $\bar{p}p$ and pp scattering is mainly due to the contribution from exchange of the M_0^J Reggeon. The experimentally observed[20,27] excess of the mean transverse momenta of the hadrons in the annihilation channels compared with the nonannihilation channels indicates a central nature of the annihilation in the plane of the impact parameters. It follows from this that the contribution from exchange of the M_0^J Reggeons [and, accordingly, the difference between the amplitudes of elastic $\bar{p}p$ and pp scattering: $\Delta T_{pp}(b) = T_{\bar{p}p}(b) - T_{pp}(b)$] in the impact-parameter representation must also be concentrated in the region of small values of the impact parameters. However, analysis of the data on the differential cross sections of elastic $\bar{p}p$ and pp scattering indicates that $\Delta T_{pp}(b)$ has a peripheral nature.[20] In Refs. 15 and 16, Rossi and Veneziano proposed to eliminate this contradiction by introducing mixing of the $\bar{q}q$ and M_0^J Reggeons. However, no calculations confirming this assumption were made. This problem is characteristic of all annihilation models in which the difference between the $\bar{p}p$ and pp interaction cross sections is related to $\bar{p}p$ annihilation. It was discussed in detail in the review of Ref. 20 by Rushbrooke and Webber in connection with models in which the annihilation channels are related to the cut of an ω Reggeon having $\bar{N}N$ structure. No solution of this problem was found in Ref. 20.

The critical remarks made above concerning the approach of Rossi and Veneziano[15,16] cannot be justified if the observed experimental dependence $\sigma_{\text{ann}}^{\bar{p}p} \propto s^{-1/2}$ is due, not to the mechanism of Fig. 3c, but to the mechanism of Fig. 3b. In this case, one cannot identify $\sigma_{\text{ann}}^{\bar{p}p}$ and $\sigma_{M_2^J}$, since, besides the cut with the annihilation channels, the diagram of Fig. 4b also has cuts with nonannihilation channels. In Sec. 3, we shall argue that the presence of a two-sheet annihilation mechanism with quark exchange leads to a negative contribution to $\Delta\sigma_{\text{tot}}^{pp}$.

To conclude the discussion of the approach of Refs. 15 and 16, we note an important omission—the role of carrier of baryon number was ascribed to a string junction. On this basis, it was assumed in Refs. 15 and 16 that the Pomeron cut leading to the string configurations M_4^J and $\bar{q}q$ does not contain annihilation channels. However, as Rossi and Veneziano themselves noted,[15,16] the string configuration M_4^J can decay into mesons as a result of $\overline{\text{SJ}}$–SJ annihilation. Thus, the Pomeron cut of the diagram can also contain annihilation events. Below, by making calculations in QCD perturbation theory, we shall show that an appreciable fraction of the cross section of $\bar{p}p$ annihilation observed at $E_{\text{lab}} \sim 10$ GeV is related to the production of M_4^J and $\bar{q}q$ string configurations corresponding to the Pomeron cut. Moreover, the energy dependence of this contribution to $\sigma_{\text{ann}}^{\bar{p}p}$ is automatically identical to the energy dependence of σ_ω.

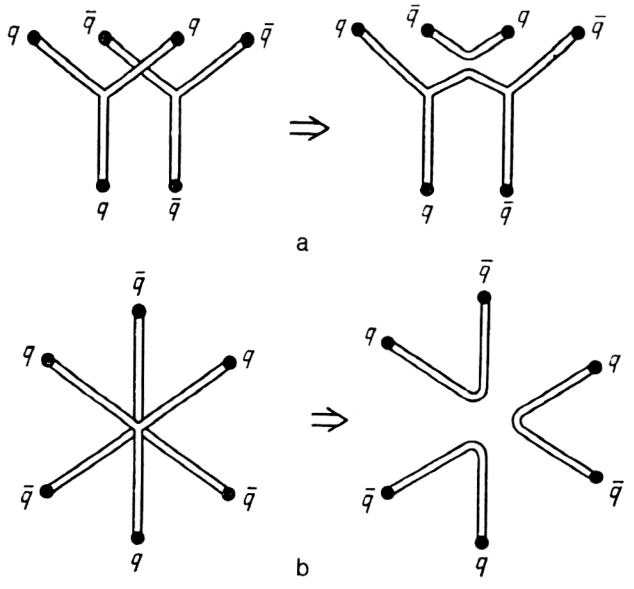

FIG. 5. Geometrical scheme of rearrangement of string configurations in the Gotsman–Nussinov model:[28] a) nonannihilation channel; b) annihilation channel.

In Ref. 28, Gotsman and Nussinov first advanced the suggestion that the cross section of $\bar{B}B$ annihilation may not decrease at asymptotic energies. Their point of departure was that the gluon fields in hadrons are localized within color strings with radius 0.2–0.3 F. In a baryon, the strings form a Y configuration, joining at a string junction. If in a collision of hadrons their color strings cross, then as a result of the change of the fields in the crossing region a rearrangement of the original string configurations of the two hadrons is possible. For example, if in a $\bar{B}B$ collision two triplet strings from the baryon and antibaryon cross, the YY configurations can go over into M_4^J and $\bar{q}q$ configurations (Fig. 5a). Processes of this type correspond to cutting of the Pomeron. If in a collision of $\bar{B}$ and B a junction and an antijunction cross, then the YY configuration can be transformed into three $\bar{q}q$ strings (Fig. 5b). Gotsman and Nussinov[28] proposed that by analogy with the Pomeron the cross section in this case too does not depend on the energy. To estimate $\sigma_{\text{ann}}^{\bar{B}B}$, they assumed that the characteristic scale of the region occupied by the string junction is of the order of the diameter of the color string. Assuming that the probability of formation of three $\bar{q}q$ strings when a junction and an antijunction cross is ~ 1, Gotsman and Nussinov[28] obtained the estimate $\sigma_{\text{ann}}^{\bar{B}B} \sim (1\text{–}2)\cdot 10^{-27}$ cm^2. Although this procedure is completely unjustified, like the analogy with the Pomeron, the conclusions of the authors and even the quantitative result were correct, as will be seen later from comparison with calculations in QCD perturbation theory.

The assumption that the annihilation cross section associated with the formation of three $\bar{q}q$ strings does not depend on the energy in the asymptotic region was also suggested by Sukhatme.[29] No serious arguments for this proposal were advanced. Sukhatme simply proceeded from intuitive considerations, assuming that the energy dependence of the cross section for the formation of any string configurations is due exclusively to quark exchanges between the baryon and the antibaryon. He noted[29] that the formation of three $\bar{q}q$ strings must be manifested in a difference between the topological cross sections of $\bar{p}p$ and pp interactions for $n \sim (3/2)\langle n \rangle$. The statistical analysis of the multiplicity distributions made below (see Sec. 2) confirms this.

Sukhatme[29] assumed that the annihilation in the asymptotic region was due to cutting of an odderon (by odderon exchange, one understands in the literature[30–33] C-odd exchange with zero flavor numbers and intercept near unity). However, a connection between the annihilation channels and the odderon cut is not supported by analysis of the graphs of QCD perturbation theory for the odderon amplitude of $\bar{B}B$ scattering in the leading logarithmic approximation. In this approximation, three gluons are joined to the baryon at the odderon–baryon interaction vertex.[34] Therefore, if the odderon is cut in the intermediate state, there is always a $3q$ system in the $\{8\}$ color state. In the nonperturbative stage of the $\bar{B}B$ interaction process, the motion of the $(3q)_{\{8\}}$ cluster must lead to the formation, in the vacuum, of a color octet tube. At breaks of this tube by the production of two $\bar{q}q$ pairs (or gluon pairs) in the fragmentation region of the initial baryon, a baryon must be produced. Thus, it can be seen that the cut of the odderon must not contain annihilation channels. This conclusion is also supported by the fact that the cross section of three-sheet events extracted from analysis of data on the difference of the topological cross sections of the $\bar{p}p$ and pp interactions, to be made below, is three orders of magnitude larger than the odderon contribution to $\Delta\sigma_{\text{tot}}^{pp}$ obtained from the elastic and total $\bar{p}p$ and pp cross sections.[32,35,36]

It can be seen from our earlier discussion of the various approaches to baryon annihilation that serious difficulties are inherent in all of them. In view of this, the search for new approaches is very important. In this review, we present the results of our recent investigations of the process of baryon annihilation[37–40] and of the $ph \to pX$ reaction with transfer of a proton to the central region of rapidities,[41] the nature of which, as will be seen below, is intimately related to the mechanisms of $\bar{p}p$ annihilation. Deferring a detailed exposition of the basic propositions of our approach to Sec. 1, we note merely that its main feature is allowance in the MQGS, by means of QCD perturbation theory, for processes with transitions of diquarks from triplet to sextet color states. These transitions lead to the formation of string configurations that are absent in the standard form of the MQGS and in which the diquarks are treated like antiquarks.

The review is divided into five sections. In Sec. 1 we present the basic assumptions of our approach to $\bar{B}B$ annihilation and classify the annihilation mechanisms associated with $D_{\{\bar{3}\}} \to D_{\{6\}}$ transitions. The dominant annihilation mechanism in the asymptotic region is associated with exchange, between the baryon and the antibaryon, of a pair of gluons in the color decuplet state.[38] The cross section of $\bar{B}B$ annihilation for this mechanism decreases weakly with

increasing energy. There also exist three preasymptotic annihilation mechanisms accompanied by gluon exchange.[40] Two of them are related by the unitarity condition to the Pomeron, and one to nonplanar corrections to secondary Reggeons. The energy dependence of the three preasymptotic mechanisms of $\bar{B}B$ annihilation is automatically the same as the energy dependence corresponding to $\bar{q}q$ Reggeons. In the case of $\bar{p}p$ annihilation, this corresponds to the dependence $\sigma_{\text{ann}}^{\bar{p}p} \propto s^{-1/2}$ observed at $E_{\text{lab}} \sim 10$ GeV.

The cross section of annihilation due to exchange of a pair of gluons in the color decuplet state for $\bar{p}p$ collisions is calculated in Sec. 2. For energies of the order of several tens of giga-electron-volts (when the production of sea $\bar{B}B$ pairs can be ignored), the contribution of this mechanism to $\sigma_{\text{ann}}^{\bar{p}p}$ must, as the calculations show, be about 10^{-27} cm^2. In the second half of Sec. 2, we analyze data on the difference between the topological cross sections in $\bar{p}p$ and pp interactions, in which production of three-sheet events in decuplet exchange in $\bar{p}p$ collisions could be manifested. The results of the analysis indicate the presence of the mechanism of formation of three-sheet events with constant cross section around 1.5×10^{-27} cm^2, in good agreement with the calculations in QCD perturbation theory.

The cross section of $\bar{N}N$ annihilation for the preasymptotic mechanisms associated with one-gluon exchange is estimated in Sec. 3. To within the theoretical uncertainties, the total contribution of the three preasymptotic mechanisms to $\sigma_{\text{ann}}^{\bar{p}p}$ agrees with the experimental data in the studied range of energies $E_{\text{lab}} < 12$ GeV. In Sec. 3, we also discuss the qualitative features of the preasymptotic annihilation mechanisms. We show that the central nature of the annihilation is a consequence of the small size of the diquark. A central nature of the annihilation for these mechanisms does not contradict the peripheral nature of $\Delta T_{pp}(b)$. In contrast, the presence of annihilation increases the extent to which $\Delta T_{pp}(b)$ is peripheral.

In Sec. 4, we consider the $ph \to pX$ process with transfer of a proton through a large rapidity interval. As in the preasymptotic annihilation mechanisms, an important part in this process is played by $D_{\{\bar{3}\}} \to D_{\{6\}}$ transitions accompanying gluon exchange. The results of the calculations agree well with the experimental data, which cannot be described in the MQGS without allowance for disintegration of the diquarks. It is shown that $D_{\{\bar{3}\}} \to D_{\{6\}}$ transitions are also important in processes of hadron production in the proton fragmentation region in ph and, especially, pA collisions. We also discuss the part played by decuplet exchange in baryon-number transfer through a large rapidity interval. These exchanges lead both to transfer of a "valence" proton (the cross section of this process is small) and baryon-number transfer through a large rapidity interval in a distinctive mechanism of production of sea $\bar{B}B$ pairs that is not present in the scheme of the $1/N$ expansion.

In Sec. 5, we discuss $\bar{p}p$ annihilation in the region of low energies, from several hundred mega-electron-volts to a few giga-electron-volts. In this region of energies, processes with annihilation of diquarks and a mechanism associated with recombination of valence quarks becomes important. The rapid growth of the $\bar{p}p$ interaction cross section with decreasing energy makes the unitarity corrections appreciable. As is expected at superhigh energies, unitarization of the scattering amplitude at low energies gives its dependence on the impact parameter the form of a "black disk." It is with this fact that the anomalously large range of the $\bar{p}p$ interaction at low energies is associated. Choice of the eikonal form of the amplitude unitarization has made it possible to describe a large set of data with high accuracy.

Section 6 is devoted to the conclusions.

1. QCD PERTURBATION THEORY AND SOFT HADRONIZATION

Two-step approach

Our treatment of $\bar{B}B$ annihilation is based on the assumption that the annihilation process can be separated into two phases. The first phase corresponds to the formation during the collision process, as a result of color exchanges, of a definite string configuration which can hadronize into purely mesonic states. The second phase includes the hadronization of this string configuration by breaking of the strings into sections. Support for the possibility of treating, in soft hadron interactions, the stage of hadronization of the color strings independently of the process of their formation is provided by the good agreement with the experimental data of Kaĭdalov's s-channel factorization relations[18] for the intercepts and slopes of secondary Reggeon trajectories. The derivation of these relations is based essentially on the assumption that the process of production of hadron states corresponding to cutting of secondary Reggeons can be separated into a stage in which a $\bar{q}q$ string is formed and a stage in which it is hadronized.

Thus, in the proposed approach the problem of determining the cross section of $\bar{B}B$ annihilation reduces to calculating the cross section for the formation of string configurations capable of breaking up into mesons (of course, with allowance for the partial probabilities of decay into mesonic states). As we have seen, in the form of the MQGS that treats diquarks as structureless objects in a $\{\bar{3}\}$ color state, there are no mechanisms capable of describing the data on $\sigma_{\text{ann}}^{\bar{p}p}$. Therefore, it can be expected that the string configurations not taken into account in the usual MQGS must be related to transitions of diquarks from triplet to sextet color states. To calculate the cross sections of the processes of formation of string configurations due to $D_{\{\bar{3}\}} \to D_{\{6\}}$ transitions, we shall use the Born approximation of QCD perturbation theory.[1)] It is obvious that the characteristic momenta of the gluons responsible for the $D_{\{\bar{3}\}} \to D_{\{6\}}$ transitions must be determined by the reciprocal scale of the diquark, since gluons with wavelength much greater than the diquark scale cannot distinguish the internal color structure of the diquark. Therefore, the conditions for applicability of QCD perturbation theory for calculations of the cross sections of such processes are more favorable than in the case of the two-gluon Pomeron model,[11,42,43] in which the characteristic momenta of the gluons are determined by the reciprocal scale of the had-

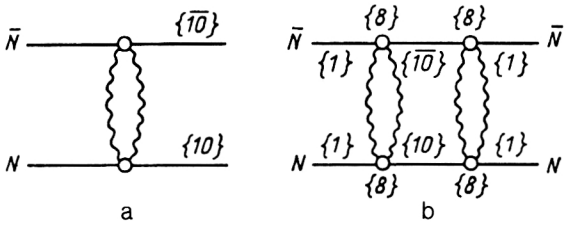

FIG. 6. Perturbation-theory diagram for the process $\bar{B}B \to (3\bar{q})_{\{\bar{10}\}} \times (3q)_{\{10\}}$, which leads in the nonperturbative stage to formation of a color decuplet string (a), and four-gluon exchange diagram having a cut with a $(3\bar{q})_{\{\bar{10}\}}(\bar{3}q)_{\{\bar{10}\}}$ intermediate state (b) and connected by the unitarity relation to diagram (a).

ron. Despite the speculative nature of the use of QCD perturbation theory ($\alpha_s \approx 0.5$–0.7), the two-gluon Pomeron model gives very reasonable quantitative results for the total cross sections,[11,42,43] the differential cross sections for elastic scattering, and the cross sections for diffraction dissociation.[43] It can therefore be hoped that the use of QCD perturbation theory will not lead to large errors in the determination of the cross sections of processes with $D_{\{\bar{3}\}} \to D_{\{6\}}$ transitions. An additional argument for this is the fact that the results of calculations of the odderon amplitude of NN scattering in the Born approximation (three-gluon exchange),[31,44,45] which, like the $D_{\{\bar{3}\}} \to D_{\{6\}}$ transition probabilities, is sensitive to the size of the diquark,[44,45] agree well with the results of phenomenological fits to the contribution of odderon exchange in NN scattering.[35,36]

The interaction with exchange of a Coulomb gluon between quarks of the baryon and antiquarks of the antibaryon occurs practically instantaneously, in contrast to the process of soft hadronization of the color strings, which requires an appreciable time.[46] Therefore, the proposed two-step approach to $\bar{B}B$ annihilation is essentially dictated by the very nature of the process. It is important that the procedure for dividing the $\bar{B}B$ annihilation process into two time phases is invariant with respect to longitudinal Lorentz transformations.

Mechanisms of $\bar{B}B$ annihilation

We first consider the annihilation mechanism that is dominant at high energies. This mechanism is associated with exchange of a pair of gluons in a color decuplet state (Fig. 6a). Since the color wave function of the $3q$ system in the color state $\{10\}$ is completely symmetric, the diagram of Fig. 6a corresponds to a process with transition of any pair of quarks in the baryon from the triplet to the sextet color state. The separation in opposite directions of the $(3q)_{\{10\}}$ and $(3\bar{q})_{\{\bar{10}\}}$ clusters in the nonperturbative stage of the $\bar{B}B$ interaction process must lead to the formation, in the vacuum, of a color decuplet tube. In the leading $1/N$ approximation, the hadronization of this tube can be represented as the hadronization of three $\bar{q}q$ strings. Thus, the mechanism of Fig. 6a can lead to three-sheet events. Because the hadronization process occurs with unit probability, the cross section calculated in QCD perturbation theory for the process $\bar{B}B \to (3\bar{q})_{\{\bar{10}\}}(3q)_{\{10\}}$ (we shall denote it by $\sigma_{\{10\}}$) can be indentified with the cross section for the three-sheet events. Up to energies of several tens of gigaelectron-volts the possible production of sea $\bar{B}B$ pairs on hadronization of the $\bar{q}q$ strings can be ignored. In this case, the cross section for production of three-sheet events is equal to the annihilation cross section.

The cross section of the $\bar{B}B \to (3\bar{q})_{\{\bar{10}\}}(3q)_{\{10\}}$ process associated with the contribution of the diagram of Fig. 6a does not depend on the energy; this, like the constancy of σ_{tot} in the two-gluon Pomeron model,[11,42,43] is a consequence of the vector nature of the gluon. Thus, the mechanism of Fig. 6a leads to a constant cross section for formation of three-sheet configurations and, accordingly, to a cross section of $\bar{B}B$ annihilation that decreases slowly with the energy (allowance for the production of sea $\bar{B}B$ pairs leads to a decrease of the annihilation cross section in accordance with the law $s^{-(0.05\text{–}0.1)}$).[37]

The diagram of Fig. 6a is related to the cut with respect to the intermediate $(3\bar{q})_{\{\bar{10}\}}(3q)_{\{10\}}$ state of the diagram of four-gluon exchange for the $\bar{B}B$ scattering amplitude (Fig. 6b). Such intermediate states are impossible for BB scattering. Naturally, this does not mean that $\sigma_{\{10\}}$ can be identified with $\Delta\sigma_{\text{tot}}^{\bar{B}B}$, since to determine $\Delta\sigma_{\text{tot}}^{\bar{B}B}$ it would be necessary to take into account all cuts for both the $\bar{B}B$ scattering amplitude and the BB scattering amplitude. At the present time, such a program has not been carried out. However, the calculations made below for the diagram of Fig. 4a show that $\sigma_{\{10\}}$ appreciably exceeds the contribution of odderon exchange to $\Delta\sigma_{\text{tot}}^{pp}$ up to ISR energies obtained by fitting experimental data on the differential and total cross sections of $\bar{p}p$ and pp scattering in phenomenological models.[32,35,36] Therefore, there are grounds for assuming that for the given mechanism of $\bar{B}B$ annihilation the Eylon–Harari hypothesis is satisfied, i.e., the annihilation cross section in the $\bar{B}B$ interactions is compensated by the cross section of the inelastic events in the BB interactions.

A feature of the soft wave function of a fast baryon is the possible appearance of a valence quark in the central rapidity region.[2–4] At the same time, the quark rapidity distribution is related to the intercept of the $\bar{q}q$ Reggeon.[2–4] The possibility of transfer of valence quarks through a large rapidity interval leads to the appearance of preasymptotic annihilation mechanisms due to the exchange of one gluon between the baryon and the antibaryon. The processes shown in Fig. 7 correspond to these mechanisms. It is assumed that the wave function of the colliding $\bar{B}B$ pair contains valence $\bar{q}D$ ($\bar{D}q$) (Fig. 7a) or $\bar{q}q$ (Fig. 7b) systems or $\bar{q}q$ annihilation (Fig. 7c). In addition, both diquarks (Figs. 7b and 7c) or one diquark (Fig. 7a) go over into a color sextet state as a result of the gluon exchange. Figure 8 shows the string configurations that must be formed in the nonperturbative stage of the $\bar{B}B$ interaction process from the final states corresponding to the diagrams of Fig. 7, which describe the first phase of the $\bar{B}B$ interaction. In representing the string configurations in Fig. 8, we have used the convenient language of triplet strings. However, we shall argue below that replacement of

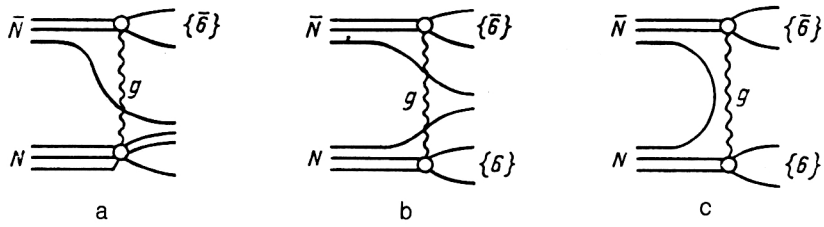

FIG. 7. Diagrams corresponding to the preasymptotic annihilation mechanisms with diquark disintegration as a result of single-gluon exchange.

the sextet string by two triplet strings is not fundamental. It is obvious that the string configuration of Fig. 8c must lead to annihilation channels if the production of sea $\bar{D}D$ pairs is ignored (which is allowed at intermediate energies). The situation with regard to the configurations of Figs. 8a and 8b is different. We shall show that for them there also exists a probability of decay into mesons.

It is clear from considerations of minimality of the string energy that the position of the string junction in the string configurations M_4^J in Figs. 8a and 8b in the rapidity scale must be near the quarks (or antiquarks). The string configurations M_4^J in Figs. 8a and 8b are strongly asymmetric and have (for the conditions that we have chosen for the rapidities of the valence quarks) a short bridge between the two string junctions. Obviously, it is possible to have a situation in which after breakings of the long ends of the strings the remaining M_4^J state is too light for production of a $\bar{B}B$ pair and decays into mesons. It is this situation that corresponds to annihilation.

A distinctive feature of all three considered preasymptotic annihilation mechanisms is that the total length of the path traversed in the scale of rapidities by the valence quarks, if string configurations that decay into mesons are to be formed, increases as $\ln s$. For this reason, the energy dependence of the annihilation cross sections for these mechanisms must have the form $\sim s^{\alpha_R(0)-1}$. In the case of $\bar{p}p$ annihilation, this corresponds to the dependence $\sigma_{\text{ann}}^{\bar{p}p} \propto s^{-1/2}$, which is observed experimentally.[2)]

The mechanisms of Figs. 7a and 7b are connected by the unitarity relation to the diagrams of Figs. 9a and 9b, which correspond to Pomeron exchange. Thus, for them the Eylon–Harari hypothesis is satisfied. In Sec. 3, we shall discuss the question of which final states in the BB interaction are associated with compensation of the annihilation channels. The diagram of Fig. 7c corresponds to symmetric cutting of the diagram of Fig. 9c, which can be regarded as a nonplanar correction to exchange of a secondary Reggeon. It is important to note that the contribution of the diagram of Fig. 9c to $\Delta\sigma_{\text{tot}}^{BB}$ need not be identical to its contribution to σ_{ann}^{BB}, since it can be cut in different ways. As will be shown in Sec. 3, its contribution to $\Delta\sigma_{\text{tot}}^{\bar{p}p}$ is negative. At the same time, $\bar{B}B$ annihilation plays the part of an absorptive correction to the bare Reggeon amplitude in the central region of impact parameters. This makes it possible to resolve the contradiction between the peripheral nature of $\Delta T_{pp}(b)$ and the central nature of $\bar{p}p$ annihilation.

In our discussion of the annihilation mechanisms, we have replaced the color strings of the higher representations ($\{10\}$ and $\{6\}$) by the triplet strings that occur in the scheme of the $1/N$ expansion. However, this simplification is not fundamental. In the case of the preasymptotic mechanisms, the color sextet strings that are produced break, like two triplet strings, when two $\bar{q}q$ pairs are produced from the vacuum. At the same time, for the diagrams of Figs. 7a and 7b we must, instead of the possibility of decay of the M_4^J states into mesons, speak of the decay into mesons of $(3q3\bar{q})$ clusters, which can be formed after the breaking of the sextet strings. The restrictions that we have chosen on the rapidities of the quarks in the mechanisms of Figs. 7a and 7b ensure in this case too the possible appearance of a light $(3q3\bar{q})$ system, which then decays into mesons. Of course, $\bar{B}B$ pairs may be produced as a result of decays of $(2q2\bar{q})$ clusters formed when a sextet string breaks up into sections. However, the probability of their decay into a $\bar{B}B$ pair must be much less than the probability of decay into mesons. First, the formation of a sufficiently heavy $(2q2\bar{q})$ cluster is improbable. For example, estimates using the probability of breaking of a triplet string, determined from the ratio Γ/M for meson resonances,[12,13] give for the mean mass of the $(2q2\bar{q})$ system a value of the order of two ρ-meson masses. Further, even if the condition $m_{(2q2\bar{q})} > 2m_B$ is satisfied, the probability of $(2q2\bar{q}) \to \bar{B}B$ decay must be small in view of the need to produce an additional $\bar{q}q$ pair and the smallness of the phase space compared with the mesonic decay modes. Therefore, the production of sea $\bar{B}B$ pairs leads merely to a slight change in the energy dependence of the contribution of the mechanisms of Fig. 7 to $\sigma_{\text{ann}}^{\bar{B}B}$. Moreover, in the case in which we are interested, $\bar{p}p$ annihilation, which has been studied up to $E_{\text{lab}} = 12$ GeV (Ref. 20), the possibility of production of sea $\bar{B}B$ pairs can be altogether ignored in view of the lowness of the energy.

For the asymptotic mechanism of $\bar{B}B$ annihilation, an

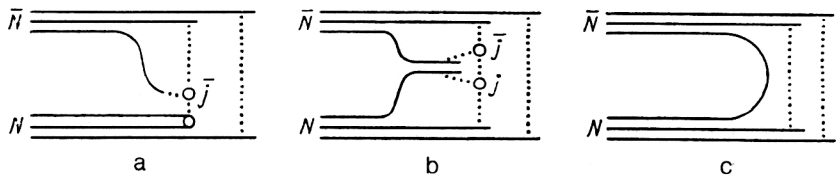

FIG. 8. String configurations formed in the nonperturbative stage of the $\bar{B}B$ interaction for the mechanisms of Figs. 7a–7c.

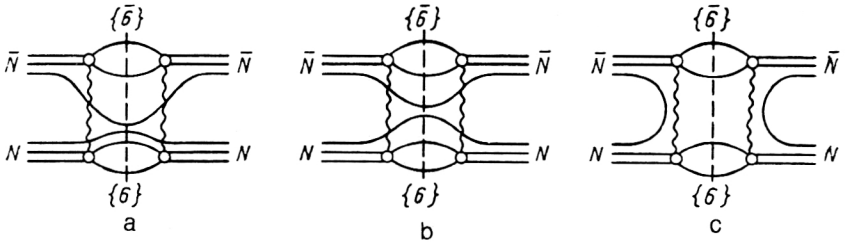

FIG. 9. Contributions to the imaginary part of the $\bar{B}B$ scattering amplitude, related by the unitarity condition to the $\bar{B}B$ annihilation mechanisms of Fig. 7.

additional source of sea $\bar{B}B$ pairs is decay of $(3q3\bar{q})$ clusters, which can be formed by breakup of a color decuplet tube. However, in this case too the small phase space for the $\bar{B}B$ mode (the mass of these clusters must be $\sim 3m_\rho$) makes decays into mesons much more probable. Therefore, even if the dynamics of the breaking of the decuplet string is very different from independent breaking of three triplet strings, the difference of the energy dependence of the contribution to $\sigma_{\text{ann}}^{\bar{B}B}$ from the mechanism of Fig. 6a must be slight.[3)] Note that this change does not have an influence on the appearance of the mechanism of Fig. 6a in the difference between the topological cross sections of the $\bar{p}p$ and pp interactions, since in this case it is not important whether the channel is an annihilation channel or not.

In view of these considerations, we shall in what follows use the language of triplet strings because of its simplicity and transparency. Moreover, the approximation of independent triplet strings is evidently quite accurate. For example, the growth, clearly expressed in $\bar{p}p$ annihilation (compared with nonannihilation), of the mean transverse momenta of the mesons with increasing Feynman variable (the "seagull" effect) finds a natural explanation if the mesons are decay products of three triplet strings (see Sec. 3).[4)]

A common property of the annihilation mechanisms associated with the diagrams of Figs. 6a and 7 is that their cross sections tend to zero with decreasing value of the ratio r_D^2/r_B^2 (r_D and r_B are the diquark and baryon radii). Thus, these annihilation mechanisms can be formally regarded as effects associated with corrections in the small parameter r_D^2/r_B^2 to the idealized MQGS with point diquarks. For a symmetric spatial wave function of the proton, $r_D^2/r_B^2 = 3/4$. However, the results of analysis of deep inelastic scattering[48–50] and large-$p_\perp$ processes[51–53] and calculations in the instanton vacuum model[54] indicate that with appreciable probability the nucleon wave function contains diquarks for which $r_D^2/r_B^2 \sim 0.1$–0.3. This circumstance significantly improves the conditions for applicability of QCD perturbation theory for analysis of the mechanisms of $\bar{N}N$ annihilation associated with the finite size of the diquark.

2. ANNIHILATION OF BARYONS AT HIGH ENERGIES

Expressions for $\sigma_{\{10\}}$

Because the color wave functions of the initial baryons in the diagram of Fig. 6a are antisymmetric, while the color wave functions of the final three-quark systems are symmetric, calculation of the diagram of Fig. 6a reduces to calculation of diagrams like that of Fig. 10. The cross section corresponding to the graphs of Fig. 10 can be expressed in the form

$$\sigma_{\{10\}}=\frac{\alpha_s^4}{2^8\pi^2}\int\prod_{i=1}^{4}\frac{d^2\mathbf{q}_i}{(q_i^2+M_g^2)}\,\delta^{(2)}\left(\sum_{j=1}^{4}\mathbf{q}_j\right)\sum_{\alpha_1,\ldots,\alpha_4=1}^{8}\times R^{\alpha_1\ldots\alpha_4}(\mathbf{q}_i,\ldots,\mathbf{q}_4)\bar{R}^{\alpha_1\ldots\alpha_4}(\mathbf{q}_1,\ldots,\mathbf{q}_4), \tag{5}$$

where

$$R^{\alpha_1\ldots\alpha_4}(\mathbf{q}_1,\ldots,\mathbf{q}_4)=\sum_{\substack{i_1\neq i_2\\ i_3\neq i_4}}\sum_{\{10\}}\langle\Psi_{STR}^{+}\Psi_C^{\{1\}}|\hat{\lambda}_{i_1}^{\alpha_1}\hat{\lambda}_{i_2}^{\alpha_2}\times\exp(i\mathbf{q}_1\mathbf{r}_{i_1}+i\mathbf{q}_2\mathbf{r}_{i_2})|\Psi_{STR}^{-}\Psi_C^{\{10\}}\rangle\times\langle\Psi_{STR}^{-}\Psi_C^{\{10\}}|\hat{\lambda}_{i_3}^{\alpha_3}\hat{\lambda}_{i_4}^{\alpha_4}\times\exp(i\mathbf{q}_3\mathbf{r}_{i_3}+i\mathbf{q}_4\mathbf{r}_{i_4})|\Psi_{STR}^{+}\Psi_C^{\{1\}}\rangle. \tag{6}$$

Here, M_g is a gluon mass introduced to take into account confinement phenomenologically; $\hat{\lambda}^\alpha$ are the Gell-Mann color matrices; α_s is the QCD coupling constant; Ψ_{STR}^{+} and Ψ_{STR}^{-} are three-quark wave functions with respect to the spin, isospin, and spatial coordinates in accordance with the Young patterns $\square\square\square$ and $\begin{smallmatrix}\square\\\square\end{smallmatrix}$; $\Psi_C^{\{1\}}$ and $\Psi_C^{\{10\}}$ are the singlet and decuplet color wave functions; $\mathbf{r}_i$ are the spatial coordinates of the quarks in the center-of-mass systems of the three-quark systems; and $\mathbf{q}_i$ are the transverse gluon momenta. The indices $i_1,\ldots,i_4$ in (6) label the quarks in the three-quark wave functions; The summation sign above the $\{10\}$ means summation over all states of the three-quark system in the color decuplet state. The expression for $R^{\alpha_1\ldots\alpha_4}$ is obtained from (6) by the substitution $\hat{\lambda}^\alpha \to (\hat{\lambda}^\alpha)^T$. Because the expressions in the matrix elements in Eq. (6) are symmetric, the summation over Ψ_{STR}^{-} in (6) can be replaced by a summation over Ψ_{STR} with an arbi-

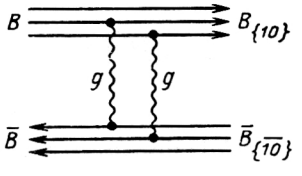

FIG. 10. Diagrams that determine the process $\bar{B}B \to (3\bar{q})_{\{\bar{10}\}}(3q)_{\{10\}}$ in the Born approximation of perturbation theory.

trary Young pattern of the three-quark system. Then (6) can be rewritten in the form

$$R^{\alpha_1\ldots\alpha_4}(\mathbf{q}_1,\ldots,\mathbf{q}_4)=\sum_{\substack{i_1\neq i_2\\ i_3\neq i_4}}\langle\Psi^+_{STR}\,|\exp\left(i\sum_{j=1}^{4}\mathbf{q}_j\mathbf{r}_{i_j}\right)|\Psi^+_{STR}\rangle$$
$$\times\sum_{\{10\}}\langle\Psi_C^{\{1\}}|\hat\lambda^{\alpha_1}_{i_1}\hat\lambda^{\alpha_2}_{i_2}|\Psi_C^{\{10\}}\rangle$$
$$\times\langle\Psi_C^{\{10\}}|\hat\lambda^{\alpha_3}_{i_3}\hat\lambda^{\alpha_4}_{i_4}|\Psi_C^{\{1\}}\rangle. \tag{7}$$

With allowance for the antisymmetry of $\Psi_C^{\{10\}}$ and the symmetry of $\Psi_C^{\{1\}}$, the expression (7) can be represented in the form

$$R^{\alpha_1\ldots\alpha_4}(\mathbf{q}_1,\ldots,\mathbf{q}_4)=6R(\mathbf{q}_1,\ldots,\mathbf{q}_4)C^{\alpha_1\ldots\alpha_4}; \tag{8}$$

$$C^{\alpha_1\ldots\alpha_4}=\sum_{\{10\}}\langle\Psi_C^{\{1\}}|\hat\lambda^{\alpha_1}_1\hat\lambda^{\alpha_2}_2|\Psi_C^{\{10\}}\rangle$$
$$\times\langle\Psi_C^{\{10\}}|\hat\lambda^{\alpha_3}_1\hat\lambda^{\alpha_4}_2|\Psi_C^{\{1\}}\rangle, \tag{9}$$

where

$$R(\mathbf{q}_1,\ldots,\mathbf{q}_4)=F(\mathbf{q}_1+\mathbf{q}_3,\mathbf{q}_2+\mathbf{q}_4,0)$$
$$+F(\mathbf{q}_1+\mathbf{q}_4,\mathbf{q}_2,\mathbf{q}_3)F(\mathbf{q}_1,\mathbf{q}_2+\mathbf{q}_3,\mathbf{q}_4)$$
$$-F(\mathbf{q}_1+\mathbf{q}_4,\mathbf{q}_2+\mathbf{q}_3,0)$$
$$-F(\mathbf{q}_1+\mathbf{q}_3,\mathbf{q}_2,\mathbf{q}_4)F(\mathbf{q}_1,\mathbf{q}_2+\mathbf{q}_4,\mathbf{q}_3). \tag{10}$$

Here, $F(\mathbf{Q}_1,\mathbf{Q}_2,\mathbf{Q}_3)$ is the three-particle form factor

$$F(\mathbf{Q}_1,\mathbf{Q}_2,\mathbf{Q}_3)=\langle\Psi^+_{STR}\,|\exp\left(i\sum_{j=1}^{3}\mathbf{Q}_j\mathbf{r}_j\right)|\Psi^+_{STR}\rangle. \tag{11}$$

For $R^{\alpha_1\ldots\alpha_4}$, the expressions (8) and (9) with the substitution $\hat\lambda^\alpha\to(\hat\lambda^\alpha)^T$ in (9) hold. It can be seen from (10) that $R(\mathbf{q}_1,\ldots,\mathbf{q}_4)$ vanishes if at least one of the gluon momenta is zero, thus ensuring infrared stability of $\sigma_{\{10\}}$. Using (10), we can also show that $R(\mathbf{q}_1,\ldots,\mathbf{q}_4)$ tends to zero if the mean distance between any quarks in the baryon tends to zero.

To calculate $\sigma_{\{10\}}$, it is necessary to know the color factor

$$C=\sum_{\alpha_1,\ldots,\alpha_4=1}^{8}C^{\alpha_1\ldots\alpha_4}\overline{C}^{\alpha_1\ldots\alpha_4}. \tag{12}$$

Calculation of the expression (12), which is given briefly in the Appendix, gives $C=160/9$. Thus, using (5) and (8), we can express $\sigma_{\{10\}}$ in the form

$$\sigma_{\{10\}}=\frac{5\alpha_s^4}{2\pi^2}\int\prod_{i=1}^{4}\frac{d^2\mathbf{q}_i}{(\mathbf{q}_i^2+M_g^2)}\,\delta^{(2)}\left(\sum_{j=1}^{4}\mathbf{q}_j\right)R^2(\mathbf{q}_1,\ldots,\mathbf{q}_4). \tag{13}$$

For the calculation of $\sigma_{\{10\}}$ in $\bar NN$ collisions, two nonrelativistic model nucleon wave functions were used. In the first case (we shall denote it by the index 1) a symmetric oscillator spatial wave function was used; for it,

$$F_1(\mathbf{Q}_1,\mathbf{Q}_2,\mathbf{Q}_3)=\exp\{-[\mathbf{Q}_1^2+\mathbf{Q}_2^2+\mathbf{Q}_3^2-\mathbf{Q}_1\mathbf{Q}_2-\mathbf{Q}_1\mathbf{Q}_3$$
$$-\mathbf{Q}_2\mathbf{Q}_3]\langle\mathbf{r}_p^2\rangle/6\} \tag{14}$$

($\langle\mathbf{r}_p^2\rangle$ is the proton mean-square electromagnetic radius). In the second case, which takes into account the possibility of dynamical enhancement in the nucleon wave function of the component with a compact *ud* diquark in the state $S=T=0$,[50–54] the wave function Ψ^+_{STR} was parametrized in the form

$$(\Psi^+_{STR})_2=A(\Psi_{1,23}+\Psi_{2,31}+\Psi_{3,12}). \tag{15}$$

Here, A is a normalization factor, and $\Psi_{i,jk}$ is the component of the wave function with quarks j and k in the state $S=T=0$. The spatial part of the wave function $\Psi_{i,jk}$ was taken in the oscillator form

$$\varphi_{i,jk}(\mathbf{r}_1,\mathbf{r}_2,\mathbf{r}_3)=\left(\frac{2\alpha}{\pi}\right)^{3/4}\left(\frac{2\beta}{\pi}\right)^{3/4}\exp(-\alpha\boldsymbol{\rho}^2-\beta\boldsymbol{\tau}^2), \tag{16}$$

$$\boldsymbol{\rho}=\mathbf{r}_i-(\mathbf{r}_j+\mathbf{r}_k)/2,\quad \boldsymbol{\tau}=\mathbf{r}_j-\mathbf{r}_k.$$

In the calculation of $F_2(\mathbf{Q}_1,\mathbf{Q}_2,\mathbf{Q}_3)$ and the normalization coefficient A in (15), we have ignored interference terms of the form $\langle\Psi_{1,23}\,|\exp(i\Sigma_j\mathbf{Q}_j\mathbf{r}_j)\,|\Psi_{2,31}\rangle$, $\langle\Psi_{1,23}|\Psi_{2,31}\rangle$. This is justified, on the one hand, by the spin–isopsin suppression of the interference terms by a factor 0.5 and, on the other, by the small value of the spatial overlap integral in the case of compact diquarks. Systematic allowance for interference terms in a nonrelativistic approach is evidently pointless, since calculations in the instanton vacuum model[54] and the fit of the baryon trajectories in the string model[55] show that the mass of the scalar *ud* diquark is ~0.2 GeV/c^2, whereas the mass of the constituent quark is ~0.3 GeV/c^2.

The values of the parameters α and β in (16) are related to the proton mean-square charge radius and the diquark mean-square radius $\langle r_D^2\rangle$:

$$\alpha=\frac{2\varepsilon^2+(1-\varepsilon)^2}{4\langle r_p^2\rangle(1-\langle r_D^2\rangle/3\langle r_p^2\rangle)},\quad \varepsilon=\left(1+\frac{m_q}{m_D}\right)^{-1},$$
$$\beta=\frac{3}{16\langle r_D^2\rangle}. \tag{17}$$

Calculation of $F_2(\mathbf{Q}_1,\mathbf{Q}_2,\mathbf{Q}_3)$ using the wave functions (15) and (16) gives

$$F_2(\mathbf{Q}_1,\mathbf{Q}_2,\mathbf{Q}_3)=\tfrac{1}{3}\{F_{1,23}+F_{2,31}+F_{3,12}\}; \tag{18}$$

$$F_{i,jk}=\exp\left\{-\frac{1}{8\alpha}[\varepsilon\mathbf{Q}_i+(1-\varepsilon)(\mathbf{Q}_j+\mathbf{Q}_k)]^2\right.$$
$$\left.-\frac{(\mathbf{Q}_j-\mathbf{Q}_k)^2}{32\beta}\right\}. \tag{19}$$

Since the nonrelativistic formalism for description of the nucleon as a bound state of a quark with $m_q\sim0.3$ GeV/c^2 and a diquark with $m_D\sim0.2$ GeV/c^2 is not, of course, justified, the expressions (18) and (19) are to be regarded as a convenient parametrization capable of reflecting the fact that the diquark is a compact object.

Results of calculations

To determine α_s 6in (13), we used the following procedure. First, we found α_s from the condition of equality of the cross section of the $NN \to N_{\{8\}}N_{\{8\}}$ process calculated in the Born approximation and the experimental cross section σ_{in}^{NN}. By σ_{in}^{NN} we understand here the cross section for inelastic interactions without allowance for the diffraction-dissociation cross section. This appears natural, since separation in opposite directions of two nucleons in the color {8} state leads to the formation, in the vacuum, of a color octet tube, with the breakings of which multiparticle hadron production is associated.[5)] In the Born approximation, $\sigma(NN \to N_{\{8\}}N_{\{8\}})$ can be calculated in accordance with the formula

$$\sigma(NN\to N_{\{8\}}N_{\{8\}})=8\pi\alpha_s^2\int\frac{d\mathbf{q}^2}{(\mathbf{q}^2+M_g^2)^2}\times[1-F(\mathbf{q})]^2, \tag{20}$$

where

$$F(\mathbf{q})=\langle N\,|\exp[i\mathbf{q}(\mathbf{r}_1-\mathbf{r}_2)]\,|N\rangle$$

is the two-quark form factor of the nucleon. The expressions for $F(\mathbf{q})$ can be obtained from the expressions (14) and (18) for $F(\mathbf{Q}_1,\mathbf{Q}_2,\mathbf{Q}_3)$ if in them we set $\mathbf{Q}_1 = \mathbf{q}$, $\mathbf{Q}_2 = -\mathbf{q}$, $\mathbf{Q}_3 = 0$. With allowance for this, calculation in accordance with (20) for wave functions 1 and 2 gives

$$\sigma_1(NN\to N_{\{8\}}N_{\{8\}})=8\pi\alpha_s^2 J\left(\frac{\langle r_p^2\rangle}{2},\frac{\langle r_p^2\rangle}{2},M_g^2\right); \tag{21}$$

$$\sigma_2(NN\to N_{\{8\}}N_{\{8\}})=\frac{8\pi\alpha_s^2}{9}[4J(a,a,M_g^2)+4J(a,b,M_g^2)+J(b,b,M_g^2)], \tag{22}$$

where

$$a=\frac{1}{8\alpha}+\frac{1}{32\beta};\quad b=\frac{1}{8\beta};$$

$$J(x,y,z)=\int_0^\infty\frac{dt(1-e^{-xt})(1-e^{-yt})}{(t+z)}.$$

In the numerical calculations, we take $\langle r_p^2\rangle^{1/2} = 0.8$ F, $M_g = m_\pi$. To determine α_s, we take $\sigma_{\text{in}}^{NN} = 30 \times 10^{-27}$ cm^2. We denote the value of α_s obtained from the condition $\sigma(NN \to N_{\{8\}}N_{\{8\}}) = \sigma_{\text{in}}^{NN}$ by the index {8}.

We find the value of α_s for the case of the diagram of Fig. 10 in accordance with the single-loop formula

$$\alpha_s^{\{10\}}=\alpha_s^{\{8\}}[\ln(\langle q\rangle_{\{10\}}/\Lambda)/\ln(\langle q\rangle_{\{8\}}/\Lambda)]. \tag{23}$$

In (23), $\langle q\rangle_{\{8\},\{10\}}$ are the mean transverse gluon momenta, which are important in the expressions (20) and (13), respectively. The value of the parameter Λ was fixed from $\alpha_s^{\{8\}}$ by means of the formula for the single-loop approximation: $\alpha_s^{\{8\}} = 6\pi/(33 - 2N_F)/\ln(\langle q\rangle_{\{8\}}/\Lambda)$. We

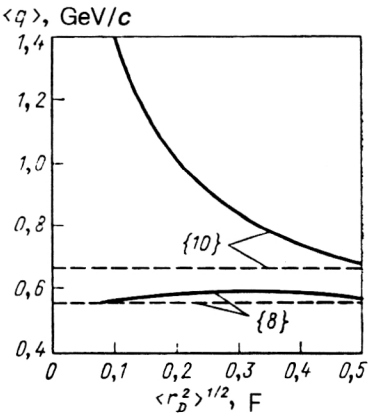

FIG. 11. Mean transverse momentum of the gluons in variant 1 ($|p\rangle = |uud\rangle$) (broken lines) and in variant 2 ($|p\rangle = |uD\rangle$) (continuous curves). The symbols {8} and {10} indicate that the averaging was performed for σ_{tot} or $\sigma_{\{10\}}$, respectively.

used two methods to determine $\langle q\rangle_{\{8\}\{10\}}$: direct calculation of $\langle q\rangle$ and determination of a "mean momentum" from the result of calculation of $\langle \ln q\rangle$. Figure 11 gives the curves for $\langle q\rangle$ in the first case. The second way of determining $q_{\{10\}}$ leads to somewhat smaller values. However, the predictions for α_s, obtained in accordance with the expression (23), which are given in Fig. 12, hardly differ from the first case.

The results of the calculations of $\sigma_{\{10\}}$ using the values of $\alpha_s^{\{10\}}$ given in Fig. 12 are shown in Fig. 13. As can be seen from Fig. 13, $\sigma_{\{10\}} \approx 1.2 \times 10^{-27}$ cm^2 for $\langle r_D^2\rangle^{1/2} \approx 0.6$ F. The cross section $\sigma_{\{10\}}$ decreases with decreasing size of the diquark, this being due to both the decrease of the integral itself in (13) and the decrease of $\alpha_s^{\{10\}}$ due to the growth of $\langle q\rangle_{\{10\}}$.

We note that the results of the calculations of $\sigma_{\{10\}}$ for variants 1 and 2 are close to each other for $\langle r_D^2\rangle^{1/2} \approx (\sqrt{3}/2)\langle r_p^2\rangle^{1/2}$, and this confirms that the interference terms are small.

In order to investigate the dependence of $\sigma_{\{10\}}$ on the choice of the value of M_g, we also made calculations for $M_g = 0$. In this case, the shape of the curves was not changed qualitatively, but the absolute values were lowered by 20–30% compared with Fig. 13. To study the dependence of $\alpha_{\{10\}}$ on $\langle r_p^2\rangle^{1/2}$ and $\varepsilon = (1 + m_q/m_D)^{-1}$, we made calculations for variant 1 with $\langle r_p^2\rangle^{1/2} = 0.7$ F and

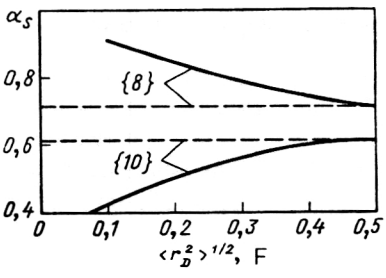

FIG. 12. Dependence of α_s in variants 1 and 2 on the diquark radius.

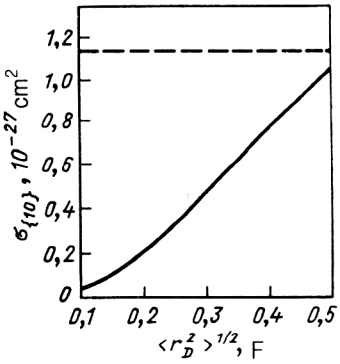

FIG. 13. Cross section of the three-sheet process $\sigma_{\{10\}}$ in variants 1 and 2.

for variant 2 with $m_D = 2m_q$. In both cases, the difference from the curves in Fig. 13 did not exceed 30–60%. Our analysis of the dependence of $\sigma_{\{10\}}$ on the choice of the model parameters offers hope that our predictions for $\sigma_{\{10\}}$ are correct up to a coefficient ~ 2.

For diquark radius ~ 0.3–0.4 F (Refs. 48–54), $\sigma^{(2)}_{\{10\}} \approx \sigma^{(1)}_{\{10\}}/2$. In this case, the resulting value of $\sigma_{\{10\}}$ is not very sensitive to the probability of finding a compact diquark in the nucleon. If this probability is ~ 0.5 (Refs. 48 and 53), then $\sigma_{\{10\}}$ must be about 10^{-27} cm^2. This value determines the cross section for the formation of three $(\bar{q}q)$ strings. To obtain from it $\sigma^{N\bar{N}}_{\text{ann}}$ at energies $E_{\text{lab}} \gtrsim 10$–$20$ GeV, when the production of $N\bar{N}$ pairs following the decay of strings is possible, it is necessary to take into account a correction factor $\exp[-(W_N/W_\pi)\langle n_\pi \rangle]$, where $W_N/W_{\pi^\pm}$ is the ratio of the probabilities of production of nucleons and pions in multiparticle production processes in the central region of rapidities, equal to ~ 0.03 for FNAL and ISR energies; $\langle n_{\pi^\pm} \rangle \sim 2\ln(s/s_0)$ is the pion mean multiplicity.

Our estimate $\sigma_{\{10\}} \sim 10^{-27}$ cm^2 signifigantly exceeds the contribution of odderon exchange to $\Delta\sigma^{pp}_{\text{tot}}$ at energies of the ISR order as determined by fitting the experimental data on the elastic and total cross sections of $\bar{p}p$ and pp interactions in phenomenological approaches.[32,35,36] Thus, for the dipole odderon model (Refs. 35 and 36) $\sigma_{\text{odd}}/\sigma_{\{10\}} \approx 10^{-3}$. In the case of the maximal odderon model (Ref. 32), $\sigma_{\text{odd}}/\sigma_{\{10\}} \approx 0.1$. Therefore, we can suppose that the three-sheet events in the $\bar{p}p$ interaction associated with the mechanism of Fig. 6a must be compensated by other channels in the pp interaction.

Analysis of data on topological cross sections

The experimental data[20] on $\sigma^{\bar{p}p}_{\text{ann}}$ are restricted to energies $E_{\text{lab}} < 12$ GeV. In this range, the cross section is $\gtrsim 10^{-26}$ cm^2 and decreases rapidly with increasing energy.[6)] However, there exist data on the difference between the topological cross sections of the $\bar{p}p$ and pp interactions,

$$\Delta\sigma_n = \sigma^{\bar{p}p}_n - \sigma^{pp}_n,$$

at $E_{\text{lab}} \sim 10$–100 GeV (Ref. 58) and $\sqrt{s} = 53$ GeV (Ref. 59).

By analyzing the data on $\Delta\sigma_n$, we shall attempt to establish whether or not there exists an energy-independent contribution of three-sheet events in the $\bar{p}p$ interactions. The hope of identifying it in $\Delta\sigma_n$ is due to the fact that its energy dependence and mean multiplicity differ appreciably from the contribution to $\Delta\sigma_n$ of the cuts of the secondary Reggeons. In view of the above-mentioned smallness of the contribution to $\Delta\sigma^{pp}_{\text{tot}}$ made by odderon exchange, it can be expected that the positive contribution to $\Delta\sigma_n$ associated with the three-sheet mechanism in the region of large multiplicities ($n \sim \frac{3}{2}\langle n \rangle_{pp}$) must be compensated by a negative contribution at moderate multiplicities. The possibility that compensation is due to events with even higher multiplicity ($n > \frac{3}{2}\langle n \rangle_{pp}$) appears unnatural for the following reason. The "tail" of the distribution with respect to n is determined by events with additional $\bar{q}q$ strings formed by the presence, in the wave function of the colliding particles, of sea $\bar{q}q$ pairs.[6,7] In view of the charge symmetry of the $\bar{q}q$ pairs in the wave function of the fast nucleon, one can expect that their influence on $\Delta\sigma_n$ at large n will be small. One can give a further argument for compensation of the positive contribution to $\Delta\sigma_n$ at $n \sim \frac{3}{2}\langle n \rangle_{pp}$ by a negative contribution at $n \sim \langle n \rangle_{pp}$. If it is assumed (on the basis of results[32,35,36] of fits to the contribution of odderon exchange to $\Delta\sigma^{pp}_{\text{tot}}$) that in QCD perturbation theory $\Delta\sigma^{pp}_{\text{tot}} \ll \sigma_{\{10\}}$ in the order α_s^4, then the contribution of the cut with respect to the intermediate state $\{10\}\{\overline{10}\}$ in the diagram of Fig. 6b must be compensated in the case of the pp scattering amplitude by the contributions of the cuts in which the $3q$ systems are in the color $\{8\}$ state. Separation of the $\{3q\}_{\{8\}}$ systems must lead to the formation of a color octet tube, i.e., to two-sheet events.

The data on $\Delta\sigma_n$ were analyzed as follows. The experimental data[58] on $\Delta\sigma_n$ for each value of n were fitted as a function of the energy by polynomials in the interval 10–100 GeV. The values that were found are shown in Fig. 14 with the errors at some energies.

Further, for fixed values of the energy the distributions $\Delta\sigma_n$ were fitted by a sum of two Gaussian distributions:

$$\Delta\sigma_n = \sum_{i=1}^{2} \frac{\alpha_i}{\beta_i}\left(\frac{\gamma_i}{\pi}\right)^{1/2} \exp\left[-\gamma_i\left(\frac{n}{\beta_i} - 1\right)^2\right]. \qquad (24)$$

It is assumed that the first term of this sum effectively corresponds to the contributions from the cutting of the ω Reggeon (the topological structure of which is very complicated and is discussed in the following section), from the above-mentioned two-sheet diagrams compensating the contribution of annihilation to $\sigma^{\bar{p}p}_{\text{tot}}$, etc. It is known (see, for example, Ref. 60) that a Gaussian parametrization gives a good description of the KNO distribution in both e^+e^- annihilation, for which $\gamma \approx 4$, and inelastic pp collisions, for which $\gamma \approx 1$.

Since the two terms in (24) correspond to diagrams with different topologies, it can be expected that

$$\frac{\gamma_2}{\gamma_1} \approx \frac{\beta_2}{\beta_1}. \qquad (25)$$

In the fits, this relation was taken as fixed.

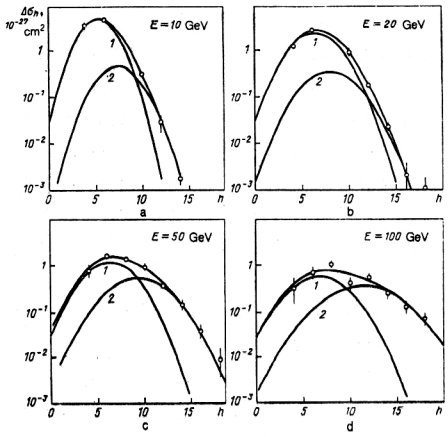

FIG. 14. Difference $\Delta\sigma_n = \sigma_n^{\bar{p}p} - \sigma_n^{pp}$ of the topological cross sections as a function of n for various energies; curves 1 and 2 show the contributions of the first and second terms in (24). The third curve corresponds to their sum.

Fits with five parameters showed that the parameter α_2, which is equal to the area under the second peak, depends weakly on the energy, whereas the parameter α_1 decreases approximately as $1/\sqrt{s}$.

Further, the set of parameters α_1 found at different energies in the interval 10–100 GeV was fitted by the energy dependence

$$\alpha_1(s) = \frac{\omega}{s^{\varphi}} - \rho. \tag{26}$$

Here, the first term corresponds to ω exchange and other contributions that decrease as $\sim 1/\sqrt{s}$. The negative, energy-independent term in (26) corresponds to the contribution of the two-sheet diagram that compensates the annihilation. We therefore imposed the requirement $\rho \approx \langle\alpha_2\rangle$, where the averaging was performed with respect to the energy. As a result, we found $\omega = 134 \times 10^{-27}$ cm^2, $\varphi = 0.56$ (this corresponds well to the difference between the $\bar{p}p$ and pp inelastic cross sections), and $\rho = 3 \times 10^{-27}$ cm^2.

After the parameter α_1 had been fitted by means of Eq. (26), the fitting procedure for each energy was repeated, now with four free parameters. The results are given in Table I and in Fig. 14, where the contributions of the first and second terms in (24) and their sum are shown separately.

It can be seen from Table I that the ratio of the mean multiplicities in the second and the first peak depends weakly on the energy and is close to the expected value $\beta_2/\beta_1 = 1.5$. The width of the peaks, determined by the parameter γ_1, also depends weakly on the energy and is close to the value $\gamma \approx 4$ observed in e^+e^- annihilation.[60]

Note that for each of the two contributions to (24) KNO scaling holds, though it is strongly violated for the total distribution in Fig. 14.

The results of the fit for the parameter α_2, which determines the area under the second peak, are the most interesting. It can be seen from Table I that α_2 depends weakly on the energy and that its mean value is $\langle\alpha_2\rangle = (3 \pm 0.2) \times 10^{-27}$ cm^2. It is natural to ascribe this contribution to the decuplet gluon exchange $\sigma_{\{10\}}$ considered above. In such a case, the value found for the cross section from the experimental data,

$$\sigma_{\{10\}}^{\bar{p}p} = (1.5 \pm 0.1) \cdot 10^{-27} \text{ cm}^2,$$

agrees quite well with the estimate obtained above in QCD perturbation theory.

Particularly interesting is the behavior of $\Delta\sigma_n$ at superhigh energies. In accordance with (26) the parameter α_1 must change sign, since the energy-independent negative contribution of the two-sheet diagram that compensates the annihilation becomes dominant. Therefore, at such en-

TABLE I. Results of a fit by means of Eq. (24) to the experimental data on the difference of the topological cross sections of multiparticle production in $\bar{p}p$ and pp collisions.

E, GeV	10	20	30	40	50	60	70	80	90	100
α_2, 10^{-27} cm^2	2,4	2,2	2,9	3,8	4,0	4,5	4,5	4,2	4,0	3,3
$\pm\Delta\alpha_2$, 10^{-27} cm^2	0,4	0,4	0,5	0,5	0,7	0,8	0,9	0,9	1,0	0,9
β_1	5,35	6,4	6,8	6,5	6,3	6,1	6,0	6,0	6,1	6,7
$\pm\Delta\beta_1$	0,05	0,1	0,1	0,2	0,3	0,4	0,4	0,5	0,7	0,8
γ_1	5,26	4,3	3,8	4,3	3,6	3,3	2,7	2,4	2,3	3,2
$\pm\Delta\gamma_1$	0,24	0,3	0,5	0,8	1,1	1,3	1,3	1,3	1,3	1,6
β_2/β_1	1,40	1,25	1,22	1,45	1,5	1,5	1,6	1,6	1,6	1,7
$\pm\Delta\beta_2/\beta_1$	0,03	0,04	0,08	0,05	0,1	0,2	0,2	0,3	0,3	0,2

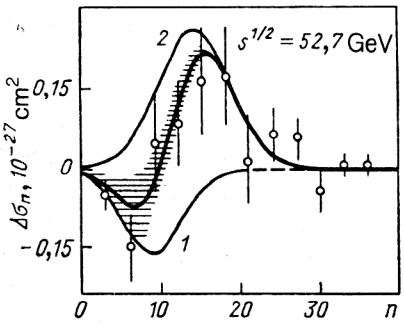

FIG. 15. The same as in Fig. 10 for energy $\sqrt{s} = 52.7$ GeV. The hatched region shows the error corridor. The data are from Ref. 59.

ergies $\Delta\sigma_n$ must become negative in the region of small n and positive at large n. Figure 15 shows ISR data[59] at c.m.s. energy $\sqrt{s} = 52.7$ GeV. They do indeed confirm the expected characteristic behavior. Moreover, using the results of the low-energy fit, we can also predict the value of $\Delta\sigma_n$. The parameter α_1 was fixed by the expression (26). We fix the parameters γ_1 and β_2/β_1 by the mean values in Table I for $E > 50$ GeV: $\gamma_1 = 2.8 \pm 0.6$, $\beta_2/\beta_1 = 1.6 \pm 0.1$. The only energy-dependent and poorly known parameter β_1 was varied. The result for $\beta_1 = 8.9 \pm 0.6$ is shown in Fig. 15.

Thus, comparison with the ISR data[59] confirms the presence of a contribution of three-sheet events with energy-independent cross section $\sim 1.5 \times 10^{-27}$ cm^2. At the same time, the ISR data[59] clearly demonstrate the compensation of the cross sections with large n in $\bar{p}p$ collisions and the cross sections with small n in pp collisions.

Also interesting is the energy dependence of the parameter β_1, which determines the mean multiplicity under the first peak. For energies $\lesssim 100$ GeV, the cross section associated with this peak must be basically determined by the contribution of the ω Reggeon [the first term in (26)]. The fit to the β_1 values given in Table I in accordance with the formula $\beta_1 = a + b \ln s$ gives $a = 3.5 \pm 0.2$ and $b = 0.85 \pm 0.7$. It is important that the parameter b, which determines the energy dependence of the mean multiplicity under the first peak, was found to be half as large as for the mean multiplicity in pp collisions. This confirms that the first peak in the intermediate range of energies corresponds to planar diagrams (ω exchange). The cylindrical diagram (Pomeron) may give nearly the same value for the mean multiplicity (this is indeed the case), owing to the relative shift in the scale of the rapidities of the two strings.[4] However, despite this the value of the parameter b must be twice as large as for the planar diagram.

3. $\bar{N}N$ ANNIHILATION AT INTERMEDIATE ENERGIES

Contribution of annihilation channels to the Pomeron

We shall give estimates of the cross sections for the three preasymptotic annihilation mechanisms listed in Sec. 1 for the case of the $\bar{N}N$ interaction. We consider first the mechanisms of Figs. 7a and 7b corresponding to cutting of the Pomeron. In the absence of a consistent theory describing the processes of formation and decay of strings, we can make only a rough estimate of the probability of decay of the string configurations M_4^J into the meson channel for the mechanisms of Figs. 8a and 8b. As restrictions on the invariant mass of the pairs $q\bar{D}$, $\bar{D}q$, $\bar{q}q$ in Figs. 8a and 8b, we take $M(\bar{q}D, \bar{D}q, \bar{q}q) \lesssim 1$ GeV/c^2. We shall assume that the probability density for decay into the annihilation channel, integrated in this range, is of order unity.

We begin by calculating the contribution to the annihilation cross section of the diagram of Fig. 7a, which we write in the form

$$\sigma_{\text{ann}}^{(7a)} = 2P_{\bar{q}D}(M)\sigma_{\{6\}}. \tag{27}$$

Here, $P_{\bar{q}D}(M)$ is the probability of finding in the initial-state wave function an $\bar{N}N$ pair of valence $\bar{q}D$ particles with invariant mass $M_{\bar{q}D} \leqslant M$; $\sigma_{\{6\}}$ is the cross section of the $\bar{D}N$ interaction that transforms the triplet $\bar{D}_{\{3\}}$ into the antisextet $\bar{D}_{\{\bar{6}\}}$. If at the same time the nucleon is treated as a qD system, then we must impose the subsidiary condition that the diquark remains in the state $D_{\{\bar{3}\}}$. The factor 2 in (27) takes into account the second diagram in Fig. 7a, which differs by the substitution $\bar{N} \rightleftarrows N$.

In the single-gluon approximation, the cross section $\sigma_{\{6\}}$ has the form

$$\begin{aligned}\sigma_{\{6\}} = \frac{\alpha_s^2}{4} \int \frac{d^2\mathbf{q}}{(\mathbf{q}^2 + M_g^2)^2} \sum_{\{6\},\{3\}} & \\ \times \langle \bar{D}_{\{3\}} \mid \sum_{i=1}^{2} (\hat{\lambda}_i^\alpha)^T e^{i\mathbf{q}\mathbf{r}_i} \mid \bar{D}_{\{\bar{6}\}} \rangle & \\ \times \langle \bar{D}_{\{\bar{6}\}} \mid \sum_{j=1}^{2} (\hat{\lambda}_j^\beta)^T e^{-i\mathbf{q}\mathbf{r}_j} \mid \bar{D}_{\{3\}} \rangle & \\ \times \langle N \mid \sum_{k=1}^{3} \hat{\lambda}_k^\alpha e^{-i\mathbf{q}\mathbf{r}_k} \mid qD_{\{\bar{3}\}} \rangle & \\ \times \langle qD_{\{3\}} \sum_{l=1}^{3} \hat{\lambda}_l^\beta e^{i\mathbf{q}\mathbf{r}_l} \mid N \rangle \,. & \end{aligned} \tag{28}$$

The summation over the spin–isospin parts of the wave functions of the states $\bar{D}_{\{\bar{6}\}}$ and $D_{\{3\}}$ can be made in (28) without allowance for the restrictions imposed by the Pauli principle, since the expressions in the matrix elements in (28) are symmetric with respect to permutations of the quarks.

The sum over the color indices of the diquarks can be written in the form

$$\sum_{\{\bar{6}\}} \langle i,j \mid \{6\} \rangle \langle \{6\} \mid k,l \rangle = \tfrac{1}{2}(\delta_k^i \delta_l^j + \delta_l^i \delta_k^j), \tag{29}$$

$$\sum_{\{3\}} \langle i,j \mid \{3\} \rangle \langle \{3\} \mid k,l \rangle = \tfrac{1}{2}(\delta_k^i \delta_l^j - \delta_l^i \delta_k^j),$$

where i, j, k, l are the color indices of the quarks.

Using these formulas and the relation

$$\langle i,j \mid \{3\}_k \rangle = \sqrt{1/2}\,\varepsilon_{ijk}, \tag{30}$$

we transform (28) to the form

$$\sigma_{\{6\}}=\frac{4\pi\alpha_s^2}{3}\int_0^\infty \frac{d\mathbf{q}^2[1-F_2^D(\mathbf{q})]}{(\mathbf{q}^2+M_g^2)^2}$$
$$\times\{\tfrac{3}{2}[1-F_2^N(\mathbf{q})F_1^D(\mathbf{q})]$$
$$+\tfrac{1}{2}[F_2^D(\mathbf{q})-F_2^N(\mathbf{q})F_1^D(\mathbf{q})]\}. \quad (31)$$

Here, $F_{1,2}^D(\mathbf{q})$ are the single- and two-quark form factors of the diquark, defined as

$$F_1^D(\mathbf{q})=\langle D_{\{3\}}|e^{i\mathbf{q}\mathbf{r}_1}|D_{\{3\}}\rangle,$$
$$F_2^D(\mathbf{q})=\langle D_{\{3\}}|e^{i\mathbf{q}(\mathbf{r}_1-\mathbf{r}_2)}|D_{\{3\}}\rangle. \quad (32)$$

In the given case, the nucleon is interpreted as a qD system, and the two-particle form factor $F_2^N(\mathbf{q})$ has the form

$$F_2^N(\mathbf{q})=\langle N|e^{i\mathbf{q}(\mathbf{r}_q-\mathbf{r}_D)}|N\rangle. \quad (33)$$

The expression (31) is infrared-stable. This is due to the fact that a long-wavelength gluon is not capable of resolving the internal structure of the diquark. Therefore, to simplify the expressions below we shall assume that $M_g=0$. Calculations show that for the choice $M_g=m_\pi$ the results are changed very little.

To calculate $F_{1,2}^D(\mathbf{q})$ and $F_2^N(\mathbf{q})$, we use a wave function of the diquark and nucleon as a qD system in the form of a nonrelativistic oscillator:

$$F_i^D(\mathbf{q})=\exp(-\alpha_i^D\mathbf{q}^2) \quad (\alpha_1^D=r_D^2/6,\ \alpha_2^D=2r_D^2/3), \quad (34)$$

$$F_2^N(\mathbf{q})=\exp(-\alpha_2^N\mathbf{q}^2) \quad (\alpha_2^N=2/3(r_p^2-r_D^2/3)). \quad (35)$$

Here, r_D^2 is the quark mean-square radius.

To calculate $F_2^N(\mathbf{q})$, we assume that the component in the nucleon wave function with $m_D\approx m_q$ is dominant.[55] However, one can show that the value of $\sigma_{\{6\}}$ is insensitive to the form of the nucleon wave function.

Substituting (34) and (35) in (31), we obtain

$$\sigma_{\{6\}}=\frac{4}{3}\pi\alpha_s^2\left\{\frac{3}{2}J(\alpha_2^{\bar D},\alpha_1^D+\alpha_2^N)\right.$$
$$\left.+\frac{1}{2}I(\alpha_2^D,\alpha_2^{\bar D},\alpha_1^D+\alpha_2^N-\alpha_2^D)\right\}, \quad (36)$$

where

$$J(a,b)=a\ln\left(\frac{a+b}{a}\right)+b\ln\left(\frac{a+b}{b}\right);$$
$$I(a,b,c)=(a+b)\ln\left(\frac{a+b+c}{a+b}\right)$$
$$+(a+c)\ln\left(\frac{a+b+c}{a+c}\right)$$
$$-a\ln\left(\frac{a+b+c}{a}\right).$$

In (36), α_i^D differs from $\alpha_i^{\bar D}$, since we intend in what follows to take into account the distribution over the size of the diquark in the nucleon.

To fix α_s in (31), we first, as in the case of the calculation of $\sigma_{\{10\}}$, determine α_s from the condition $\sigma(NN\to N_{\{8\}}N_{\{8\}})=\sigma_{\text{in}}$ (for $M_g=0$, this leads to $\alpha_s\approx 0.5$). Then, using the single-loop formula, we take into account the change in α_s due to the change in the mean momenta of the gluons on the transition from the case $\sigma(NN\to N_{\{8\}}N_{\{8\}})$ to the case $\sigma_{\{6\}}$ (allowance for this may be important if the diquark has a small radius).

We make all the calculations with two types of nucleon wave function. In the first case (denoted by I), we set $r_D=0.7$ F, and this corresponds to a symmetric oscillator wave function of the nucleon. In the second case (II), we assume the existence of a 50% admixture of a component with a compact diquark[48–53] with $r_D=0.4$ F. In these two cases,

$$\sigma_{\{6\}}\approx\begin{cases}0.31\sigma_{\text{in}}^{NN}\approx 9\cdot 10^{-27}\ \text{cm}^2\ \text{(I)},\\ 0.23\sigma_{\text{in}}^{NN}\approx 7\cdot 10^{-27}\ \text{cm}^2\ \text{(II)}.\end{cases} \quad (37)$$

Here and in what follows, the upper and lower values correspond to the calculations in the variants I and II.

Further, to calculate the annihilation cross section (27), we must estimate the probability $P_{\bar qD}(M)$. We use the following parametrization for the distribution of $\bar q$ in $\bar N$ with respect to the variable $x_+=\frac{1}{2}(x+(x^2+x_\perp^2)^{1/2})$, where $x_\perp^2=4m_\perp^2/s$, $m_\perp^2=m_q^2+\langle p_{q\perp}^2\rangle$:

$$f_{\bar q}(x_+)=Cx_+^{-\alpha_R(0)}(1-x_+)^{\beta-1}. \quad (38)$$

Here, $\beta=1+\alpha_R(0)-2\alpha_N(0)$, $\alpha_R(0)=0.5$, $\alpha_N(0)=-0.5$.

The normalization factor C is fixed by the condition of unit probability of finding a q in the nucleon:

$$C^{-1}=\frac{\Gamma[1-\alpha_R(0)]\Gamma(\beta)}{\Gamma[\beta-\alpha_R(0)+1]}$$
$$-\frac{1}{1-\alpha_R(0)}\left(\frac{m_q^2+p_{q\perp}^2}{s|x_q^{\min}|}\right)^{1-\alpha_R(0)} \quad (39)$$

Here, $x_q^{\min}$ is the minimal value of the Feynman variable of the antiquark transferred to the fragmentation region of the nucleon (we assume $x_{\bar N}=1$). In this region, the configurations with a leading diquark are predominant, and therefore we set $x_{\bar q}^{\min}\approx -0.5$. Unfortunately, it is not yet possible to describe correctly the system $\bar qqD$ and, in particular, the correlations of their momenta in the nucleon fragmentation region. Nevertheless, (39) depends weakly on $x_{\bar q}^{\min}$ and qualitatively gives a correct reflection of the decrease of the phase space of the quarks in the initial $\bar NN$ interactions with decreasing energy.

We rewrite (38) as $x_+\to 0$ in the scale of rapidities in the center-of-mass system:

$$W_{\bar q}(y_{\bar q})=C((m_\perp/\sqrt{s})e^y)^{1-\alpha_R(0)}. \quad (40)$$

Ignoring the correlation of the $\bar q$ and D momenta, we write the probability $P_{\bar qD}(M)$ in the form

$$P_{\bar{q}D}(M)=\int_{y_{\bar{q}}^{\min}+\delta(M)}^{y_{\bar{p}}^{\min}} dy W_{\bar{q}}(y), \tag{41}$$

where

$$\delta(M)=\operatorname{arch}((M^2-m_{q\perp}^2-m_{D\perp}^2)/(2m_{q\perp}m_{D\perp})). \tag{42}$$

The minimal value of the antiquark rapidity $y_{\bar{q}}^{\min}$ can be determined from the condition $(m_q + m_D) \times \exp|y_{\bar{q}}^{\min}|/\sqrt{s} \approx 1$, which, in its turn, follows from the requirement that the Feynman variable of the $\bar{q}D$ system be bounded: $|x_{\bar{q}D}| < 1$ [with allowance for the leading diquark in the momentum distribution in the nucleon we assume in (41) that $|y_D| > |y_{\bar{q}}|$].

Setting $M = 1$ GeV/c^2 and $m_{q\perp} \approx m_{D\perp} \approx 0.3$ GeV/c^2 (Refs. 54 and 55), we obtain

$$P_{\bar{q}D}(M=1\ \text{GeV}/c^2)\approx 1.7\sqrt{s_0/s},$$
$$s_0=1\ \text{GeV}^2. \tag{43}$$

Substituting (37) and (43) in (27), we obtain the annihilation cross section (cm^2):

$$\sigma_{\text{ann}}^{(7a)}\approx\begin{cases}30\cdot10^{-27}\sqrt{s_0/s}\,(\text{I}),\\ 24\cdot10^{-27}\sqrt{s_0/s}\,(\text{II}).\end{cases} \tag{44}$$

We now turn to the diagram of Fig. 7b. We write the contribution to the annihilation cross section in a form analogous to (27):

$$\sigma_{\text{ann}}^{(7b)}\approx P_{\bar{q}q}(M)\sigma_{\{\bar{6},6\}}. \tag{45}$$

Here, $P_{\bar{q}q}(M)$ is the probability of a fluctuation in the wave function of the system of the colliding $\bar{N}N$ in which the valence pair $\bar{q}q$ has mass $M_{\bar{q}q} \leqslant M$; $\sigma_{\{\bar{6},6\}}$ is the cross section of the process $\bar{D}_{\{\bar{3}\}}D_{\{\bar{3}\}} \to \bar{D}_{\{\bar{6}\}}D_{\{6\}}$ averaged over the triplet color indices of the initial $\bar{D}_{\{\bar{3}\}}$ and $D_{\{3\}}$:

$$\sigma_{\{\bar{6},6\}}=\frac{1}{9}\sum_{n,m=1}^{3}\sigma_{\{\bar{6},6\}}^{n,m}, \tag{46}$$

where

$$\sigma_{\{\bar{6},6\}}^{n,m}=\frac{\alpha_s^2}{4}\int\frac{d^2\mathbf{q}}{\mathbf{q}^4}\sum_{\{6\},\{\bar{6}\}}\langle D_{\{\bar{3}\}_n}|\sum_{i=1}^{2}\hat{\lambda}_i^{\alpha}e^{i\mathbf{q}\mathbf{r}_i}|D_{\{6\}}\rangle$$
$$\times\langle D_{\{6\}}|\sum_{j=1}^{2}\hat{\lambda}_j^{\beta}e^{-i\mathbf{q}\mathbf{r}_j}|D_{\{\bar{3}\}_n}\rangle$$
$$\times\langle\bar{D}_{\{\bar{3}\}_m}|\sum_{k=1}^{2}(\hat{\lambda}_k^{\alpha})^T e^{i\mathbf{q}\mathbf{r}_k}|\bar{D}_{\{\bar{6}\}}\rangle$$
$$\times\langle\bar{D}_{\{\bar{6}\}}|\sum_{l=1}^{2}(\hat{\lambda}_l^{\beta})^T e^{i\mathbf{q}\mathbf{r}_l}|\bar{D}_{\{\bar{3}\}_m}\rangle. \tag{47}$$

The summation over the spatial and spin–isospin parts of the $D_{\{6\}}$ and $\bar{D}_{\{\bar{6}\}}$ wave functions can be taken, as in (28), without allowance for the Pauli principle. Bearing in mind also that the color wave function of the state $\{\bar{3}\}$ is antisymmeric, while that of the state $\{6\}$ is symmetric, we write (47) in the form

$$\sigma_{\{\bar{6},6\}}^{n,m}=\frac{\pi\alpha_s^2}{4}C_{nm}\int_0^{\infty}\frac{d\mathbf{q}^2}{(\mathbf{q}^2+M_g^2)^2}$$
$$\times[1-F_2^D(\mathbf{q})][1-F_2^{\bar{D}}(\mathbf{q})]. \tag{48}$$

The factor C_{nm} can be calculated using (29) and (30):

$$C_{nm}=5+9\delta_{nm}. \tag{49}$$

As in the case of $\sigma_{\{6\}}$, the expression (48) for $\sigma_{\{\bar{6},6\}}$ is infrared-stable, and this enables us to set $M_g = 0$. Using the same procedure to normalize α_s as in the calculation of $\sigma_{\{6\}}$, and making calculations in accordance with Eq. (48), we obtain

$$\sigma_{\{\bar{6},6\}}=\begin{cases}8\cdot10^{-27}\ \text{cm}^2\ (\text{I}),\\ 5\cdot10^{-27}\ \text{cm}^2\ (\text{II}).\end{cases} \tag{50}$$

Further, the factor $P_{\bar{q}q}(M)$ in (45) can be estimated in accordance with the formula

$$P_{\bar{q}q}(M)=\int_{|y_{q,\bar{q}}|<Y}W_{\bar{q}}(y_{\bar{q}})W_q(y_q)$$
$$\times\theta(\varepsilon-|y_q-y_{\bar{q}}|)dy_{\bar{q}}dy_q, \tag{51}$$

where $\varepsilon = 2\cosh^{-1}(M/2m_{q\perp})$, $W_{\bar{q}}(y)$ is determined in (40), $W_q(y) = W_{\bar{q}}(-y)$, $Y = \ln(x_0\sqrt{s}/m_{\perp})$, and $x_0 \approx 1/3$. The factor x_0 arises naturally on replacement of the smooth distribution (38) in the nucleon fragmentation region by the expression (40) in the rapidity scale.

The integral (51) can be calculated by changing the variables of integration to $(y_{\bar{q}} \pm y_q)$. We take into account the restriction $|y_{q,\bar{q}}| < Y$ approximately, reducing the limits of integration with respect to the variable $(y_{\bar{q}} + y_q)/2$ by the amount $\langle|\Delta y|\rangle$, the mean value of the rapidity interval between the $\bar{q}$ and the q:

$$\langle|\Delta y|\rangle=\int_{-\varepsilon}^{\varepsilon}d\Delta y\Delta y\exp[(1-\alpha_R(0))\Delta y]$$
$$\times\left[\int_{-\varepsilon}^{\varepsilon}d\Delta y\exp[(1-\alpha_R(0))\Delta y]\right]^{-1}. \tag{52}$$

Carrying out the procedure of the calculations described above, we find

$$P_{\bar{q}q}(M)$$
$$=4C\left(\frac{M^2-4m_{q\perp}^2}{s}\right)^{1/2}$$
$$\times\left\{\ln\left(\frac{2x_0\sqrt{s}}{M+(M^2-4m_{q\perp}^2)^{1/2}}\right)+\left(\frac{M-2m_{q\perp}}{M+2m_{q\perp}}\right)^{1/2}\right\}. \tag{53}$$

Finally, combining (45), (50), and (53), we find the contribution of the diagram of Fig. 7b to the cross section of $\bar{N}N$ annihilation (cm^2):

$$\sigma_{\text{ann}}^{(7b)}\approx\begin{cases}28\cdot10^{-27}\sqrt{s_0/s}\ (\text{I}),\\ 18\cdot10^{-27}\sqrt{s_0/s}\ (\text{II}).\end{cases} \tag{54}$$

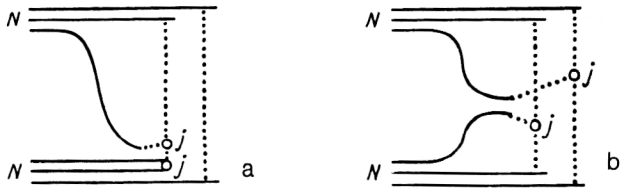

FIG. 16. String configurations formed in NN collisions that are related to compensation of annihilation channels in NN collisions that are part of the Pomeron cut (see Figs. 7a and 7b).

It can be seen from (44) and (54) that the total contribution of the diagrams of Figs. 7a and 7b explains an appreciable fraction of the experimentally observed annihilation cross section.

As we have already said, the contribution of the diagrams of Figs. 7a and 7b to the total cross section of the $\bar{N}N$ interaction—it is shown in Figs. 8a and 8b—is part of the Pomeron, i.e., it satisfies the Eylon–Harari hypothesis.[23] The corresponding part of the Pomeron contribution to the NN interaction cross section is related by the unitarity condition to the processes shown in Figs. 16a and 16b. These NN interaction channels, compensating the annihilation contributions of the mechanisms of Figs. 7a and 7b to the difference $\Delta\sigma_{\text{tot}}^{NN}$ between the total cross sections, correspond to production of an NN pair with low effective mass in the region of fragmentation of one of the nucleons (Fig. 16a) or in the central region (Fig. 16b).

Nonplanar annihilation corrections to the Reggeons

We now consider the annihilation mechanism with quark exchange (see Fig. 7c). In this mechanism, there is formed a combination of two $\bar{q}q$ strings (see Fig. 8c), which decay mainly into mesons. Therefore, there is no need to estimate the partial probabilities of decay into mesons, as there was for the annihilation mechanisms associated with the Pomeron cut. However, it is difficult to estimate the annihilation cross section of the corresponding diagram in Fig. 7c because of the absence of a consistent dynamical scheme for the $\bar{q}q$ Reggeons. We shall estimate the contribution of the annihilation cut of the diagram of Fig. 9c to $\sigma_{\text{ann}}^{\bar{N}N}$ under two different assumptions concerning the structure of the Reggeon exchange; we call them A and B.

In variant A, we shall assume that the quarks exchanged by the hadrons emit and absorb gluons and that this process is described by a planar diagram.[61]

In variant B, we shall assume that the quark color index does not change along the quark line; gluons are not emitted. Quark exchange distinguishes a certain rare configuration in the nucleon wave function.[46,62]

In variant A, in the leading $1/N$ approximation we can ignore the change of the triplet color indices of the $\bar{D}$ and D after the two-gluon exchange in the diagram of Fig. 9c. We write the contribution to the $\bar{N}N$ scattering amplitude from the diagram of Fig. 9c in the form

$$\Delta_{\{\bar{6},6\}}T_R(b) = -\Gamma_{\{\bar{6},6\}}(b)T_R^0(b). \tag{55}$$

Here, $\Gamma_{\{\bar{6},6\}}(b)$ is the profile function of the elastic amplitude of $\bar{D}D$ scattering, calculated in the two-gluon approximation with the intermediate state $\{\bar{6}\}$–$\{6\}$. The notation $\Delta_{\{\bar{6},6\}}T_R(b)$ emphasizes the fact that this is a correction to the bare Regge amplitude T_R^0. In (55) it is assumed that the centers of mass of the nucleon and diquark in the impact-parameter plane coincide, since the latter carries most of the nucleon momentum.

We parametrize the functions $\Gamma_{\{\bar{6},6\}}(\mathbf{b})$ and $T_R^0(\mathbf{b})$ in the Gaussian form

$$\Gamma_{\{\bar{6},6\}}(\mathbf{b}) = (\sigma_{\{\bar{6},6\}}/8\pi\lambda_{\{\bar{6},6\}})\exp(-\mathbf{b}^2/4\lambda_{\{\bar{6},6\}}); \tag{56}$$

$$T_R^0(\mathbf{b}) = T_R^0(0)\exp(-\mathbf{b}^2/4\lambda_R). \tag{57}$$

The parameter $\lambda_{\{\bar{6},6\}}$ can be estimated as $\lambda_{\{\bar{6},6\}} \approx r_D^2/3$. The exact value of $\lambda_{\{\bar{6},6\}}$ is not important, since the diquark radius is small compared with the interaction range in Reggeon exchange.

We rewrite (55) in the momentum representation for $q=0$ in the form

$$\Delta_{\{\bar{6},6\}}T_R(q=0) = -K_{\{\bar{6},6\}}^R T_R^0(q=0),$$

where

$$K_{\{\bar{6},6\}}^R = \sigma_{\{\bar{6},6\}}/8\pi(\lambda_R + \lambda_{\{\bar{6},6\}}). \tag{58}$$

It follows from phenomenological analysis[63] of data at energies 10–20 GeV that $\lambda_\omega \approx 11$ $(\text{GeV}/c)^{-2}$, $\lambda_f \approx 5$ $(\text{GeV}/c)^{-2}$. Accordingly, from (50) and (58) we obtain

$$K_{\{\bar{6},6\}}^f \approx \begin{cases} 0.1 \text{ (I)} \\ 0.066 \text{ (II)} \end{cases}, \tag{59}$$

$$K_{\{\bar{6},6\}}^\omega \approx \begin{cases} 0.065 \text{ (I)} \\ 0.045 \text{ (II)} \end{cases}. \tag{60}$$

This correction to the Reggeon contribution to the scattering amplitude can be related to the annihilation cross section by means of the AGK cutting rules:[64]

$$\sigma_{\text{ann}}^{(7b)} = 2K_{\{\bar{6},6\}}^f \sigma_f^0 + 2K_{\{\bar{6},6\}}^\omega \sigma_\omega^0. \tag{61}$$

To calculate the annihilation cross section, it is now necessary to estimate the bare Reggeon contributions σ_f^0 and σ_ω^0 to the total cross section. We begin with σ_ω^0. From the experimental data only the effective ω-Reggeon contribution is known:

$$\Delta\sigma_{\text{tot}}^{pp} = 2\sigma_\omega^{\text{eff}} = 2(\sigma_\omega^0 - \sigma_\omega^{\text{abs}}), \tag{62}$$

where $\sigma_\omega^{\text{abs}}$ includes not only $\Delta_{\{\bar{6},6\}}\sigma_\omega$ but other corrections, considered below.

The presence of sea gluons makes possible also the intermediate diquark states $\{\bar{6}\}$–$\{\bar{3}\}$ and $\{3\}$–$\{6\}$ in Fig. 9c. However, in contrast to the $\{\bar{6}\}$–$\{6\}$ state, considered above, these corrections do not contribute to the annihilation and are connected by the unitarity relation to processes in which a nucleon or an antinucleon is transferred to the central region. The screening correction to the bare amplitude T_ω^0 due to the graph of Fig. 9c with intermediate diquark states $\{\bar{6}\}$–$\{\bar{3}\}$ and $\{3\}$–$\{6\}$ can be calculated in accordance with Eq. (58) with replacement of $\sigma_{\{\bar{6},6\}}$ by $2\sigma_{\{3,6\}}$. We write the cross section of the process

$\bar{D}_{\{3\}}D_{\{\bar{3}\}} \to \bar{D}_{\{\bar{6}\}}D_{\{\bar{3}\}}$, averaged over the color indices of the initial states, in the form

$$\sigma_{\{3,6\}}=\frac{\alpha_s^2}{36}\sum_{n,m}\int\frac{d^2\mathbf{q}}{(\mathbf{q}^2+M_g^2)^2}\sum_{\{6\},\{3\}}$$
$$\times\langle\bar{D}_{\{3\}_n}|\sum_{i=1}^{2}\hat{\lambda}_i^{\alpha}e^{i\mathbf{q}\mathbf{r}_i}|\bar{D}_{\{\bar{6}\}}\rangle$$
$$\times\langle\bar{D}_{\{\bar{6}\}}|\sum_{j=1}^{2}\hat{\lambda}_j^{\beta}e^{i\mathbf{q}\mathbf{r}_j}|\bar{D}_{\{3\}_n}\rangle$$
$$\times\langle D_{\{\bar{3}\}_m}|\sum_{k=1}^{2}(\hat{\lambda}_k^{\alpha})^T e^{-i\mathbf{q}\mathbf{r}_k}|D_{\{\bar{3}'\}}\rangle$$
$$\times\langle D_{\{\bar{3}'\}}\sum_{l=1}^{2}(\hat{\lambda}_l^{\beta})^T e^{-i\mathbf{q}\mathbf{r}_l}|D_{\{\bar{3}\}_m}\rangle\,. \qquad (63)$$

Here, we are forced to retain the gluon mass M_g, which takes into account confinement effectively, since the expression for $\sigma_{\{3,6\}}$, in contrast to $\sigma_{\{6\}}$ and $\sigma_{\{\bar{6},6\}}$, is infrared-divergent.

Using the relations (29) and (30), we rewrite (63) in the form

$$\sigma_{\{3,6\}}=\frac{2\pi\alpha_s^2}{3}\int_0^{\infty}\frac{d\mathbf{q}^2}{(\mathbf{q}^2+M_g^2)^2}$$
$$\times[1+F_2^D(\mathbf{q})][1-F_2^{\bar{D}}(\mathbf{q})]. \qquad (64)$$

Setting here for simplicity $F_2^D(\mathbf{q}) = F_2^{\bar{D}}(\mathbf{q})$ and using the parametrization (34), we find

$$\sigma_{\{3,6\}}=\frac{8}{9}\pi\alpha_s^2 r_D^2\exp\left(\frac{4}{3}r_D^2M_g^2\right)\mathrm{Ei}\left(-\frac{4}{3}r_D^2M_g^2\right). \qquad (65)$$

Fixing $M_g = m_\pi$, we obtain $\alpha_s = 0.7$ from the normalization on $\sigma_{\text{in}}^{\bar{N}N}$. Then from (58) and (65) we have

$$K_{\{3,6\}}^{\omega}=\begin{cases}0.14\ (\text{I}),\\ 0.1\ (\text{II}).\end{cases} \qquad (66)$$

In addition, there are corrections from the ordinary $\omega^{\mathbf{P}}$ branchings (without disintegration of the triplet diquarks), which give $K^{\omega P}\approx 0.25$. Adding here (60) and (66), we find from (62) the relative contribution of the bare ω Reggeon:

$$\sigma_{\omega}^{0}/\Delta\sigma_{\text{tot}}^{pp}=\begin{cases}0.9\ (\text{I}),\\ 0.83\ (\text{II}).\end{cases} \qquad (67)$$

The relation between the bare f and ω Reggeons depends on the degree of violation of the exchange degeneracy. The fit to the experimental data in the quasi-eikonal model[63] gives strong violation: $\sigma_f/\sigma_\omega \approx 2.7$. In this case, the contribution of the mechanism corresponding to Fig. 7c in variant A is, in accordance with (59)–(61),

$$(\sigma_{\text{ann}}^{(7b)}/\Delta\sigma_{\text{tot}}^{pp})_{\text{A}}\approx\begin{cases}0.6\ (\text{I}),\\ 0.36\ (\text{II}).\end{cases} \qquad (68)$$

In variant B, accompanying gluons are absent, and therefore in the intermediate state in Fig. 9c only the system $\{\bar{6}\}$–$\{6\}$ is possible. Another difference from variant A is the color factor 7/4, which must be introduced on the right-hand side of the expression (58). This can be seen by using Eq. (49) for the coefficients C_{nm}. A procedure analogous to the one for variant A leads to the estimate

$$(\sigma_{\text{ann}}^{(7b)}/\Delta\sigma_{\text{tot}}^{pp})_{\text{B}}\approx\begin{cases}0.95\ (\text{I}),\\ 0.55\ (\text{II}).\end{cases} \qquad (69)$$

It should be emphasized that the estimates (68) and (69) have a theoretical uncertainty of about 100%. For example, they depend strongly on the degree of violation of the ω–f exchange degeneracy. The phenomenological approach of Ref. 65, based on calculations[66] of the Pomeron amplitude in QCD perturbation theory, describes well the accelerator and cosmic-ray data on the total cross sections and recently obtained data of the $S\bar{p}pS$ collider for the phase of elastic scattering. The results of the analysis demonstrate a weak violation of the exchange degeneracy: $\sigma_f/\sigma_\omega \approx 1.2$. In such a case, the values of the quantities on the right-hand sides of (68) and (69) should be halved.

Bearing in mind that experimentally $\sigma_{\text{ann}}^{\bar{p}p} \approx \Delta\sigma_{\text{tot}}^{pp}$, we see from (68) and (69) that the mechanism of Fig. 7c can make a significant contribution to the cross section of $\bar{p}p$ annihilation in the region of intermediate energies. It is interesting that the presence of this annihilation mechanism not only increases $\Delta\sigma_{\text{tot}}^{pp}$ but, in contrast, leads to a negative contribution to the difference between the $\bar{p}p$ and pp interaction cross sections.

Discussion of the results of analysis of the preasymptotic mechanisms of $\bar{N}N$ annihilation

Adding the estimates (44), (54), and (68) [or (69)], we see that the mechanisms associated with the diagrams of Figs. 7a, 7b, and 7c make a contribution to the $\bar{p}p$ annihilation cross section that agrees qualitatively with the experimental data for $E_{\text{lab}} \lesssim 12$ GeV $[(\sigma_{\text{ann}}^{\bar{p}p})_{\text{exp}} \simeq C(s_0/s)^{0.56}$, $C \approx 70\times10^{-27}$ cm^2, $s_0 = 1$ GeV^2 (Ref. 20)]. From the point of view of the considered mechanisms, the experimentally observed approximate equality of $\sigma_{\text{ann}}^{\bar{p}p}$ and $\Delta\sigma_{\text{tot}}^{\bar{p}p}$ appears fortuitous. Indeed, a decrease in the size of the diquark leads to a decrease of $\sigma_{\text{ann}}^{\bar{p}p}$ but hardly affects $\Delta\sigma_{\text{tot}}^{pp}$. However, it is important that the energy dependence of the annihilation cross section for the mechanisms of Figs. 7a, 7b, and 7c must be the same as the energy dependence of $\Delta\sigma_{\text{tot}}^{pp}$. It should be said that experimentally, besides the relation $\sigma_{\text{ann}}^{\bar{p}p} \approx \Delta\sigma_{\text{tot}}^{pp}$, for $n \gtrsim 4$ the stronger relation $(\sigma_{\text{ann}}^{\bar{p}p})_n \approx \Delta\sigma_n$ is also satisfied quite well.[20,67] Correct analysis of the ratio of $(\sigma_{\text{ann}}^{\bar{p}p})_n$ to $\Delta\sigma_n$ in the proposed scheme at energies 10–20 GeV is hardly possible, since the energies of the individual strings are low, and the natures of the final hadron states, which are different in $\bar{p}p$ and pp interactions, have a strong influence on the multiplicity distributions.

It is important to note that the three preasymptotic annihilation mechanisms considered above make it possible to solve the old problem, already mentioned, of the apparent contradiction between the central nature of $\bar{p}p$ annihilation and the peripheral nature of the difference between the $\bar{p}p$ and pp scattering amplitudes $[\Delta T_{pp}(b)]$ in the impact-parameter plane.[20] Indeed, the mechanisms of $\bar{p}p$ an-

nihilation associated with cutting of the Pomeron do not contribute to $\Delta T_{pp}(b)$. As can be seen from (55) and (56), the general effect of the mechanism of Fig. 7c reduces to an additional screening of the bare Reggeon amplitude in the central region of impact parameters ($b \lesssim r_D$), and this makes $\Delta T_{pp}(b)$ even more peripheral.[7)] At the same time, the central nature of the annihilation is explained by the fact that for all three mechanisms the $D_{\{\bar{3}\}} \to D_{\{6\}}$ transition probabilities are not small only for central collisions with values of the impact parameter satisfying $b \lesssim r_D$ (we recall that in the b plane the diquark center of mass is close to the nucleon center of mass, since almost the entire longitudinal momentum of the nucleon is concentrated on the diquark). In contrast to the annihilation channels, in nonannihilation inelastic interactions the characteristic values of the impact parameter are determined, not by the size of the diquark, but by the size of the nucleon, and this makes them more peripheral.

In the analysis of the experimental data, the conclusion of a more central nature of the annihilation events compared with the nonannihilation events is deduced from the fact that the mean transverse momenta of the hadrons in the first case are greater than in the second.[20] From the point of view of the mechanisms of Fig. 7, this difference must be due to the higher transverse momentum of the ends of the strings for the configurations of Fig. 8 compared with the string configurations of the nonannihilation events, which are not accompanied by disintegration of the diquarks. This is a consequence of the fact that the momentum of the gluons and the Fermi momentum of the quarks in the diquark, from which the transverse momentum of the ends of the strings is made up, are determined for the annihilation mechanisms by the reciprocal diquark radius, while in the case of the nonannihilation events without disintegration of the diquarks the momentum of the gluon and the Fermi momentum of the quarks (or diquarks) in a nucleon are determined by the reciprocal nucleon radius. The presence, in the nucleon wave function, of a component with a compact *ud* diquark can have an important influence on this effect.[48–53]

The enhanced value of $\langle p_\perp \rangle$ in annihilation events is usually[20] explained by the fact that the annihilation is associated with multiperipheral diagrams involving exchange of baryons with $m \simeq 1$ GeV/c^2. However, the multiperipheral model cannot explain the dependence of $\langle p_\perp \rangle$ on the Feynman variable x. A characteristic feature of the annihilation events in $\bar{p}p$ interactions at $p_{\text{lab}} \lesssim 12$ GeV/c (Ref. 20) is the rapid growth of $\langle p_\perp \rangle$ with increasing x. The transverse momentum varies from $\langle p_\perp \rangle \approx 0.2$–$0.3$ GeV/c at $x \approx 0$ to $\langle p_\perp \rangle \approx 0.8$–$0.9$ GeV/c at $x \gtrsim 0.5$. Somewhat less growth of $\langle p_\perp \rangle$ with x was also observed in the exclusive annihilation channels in $\bar{p}p$ annihilation at $p_{\text{lab}} = 32$ GeV/c.[27] As is well known,[68] growth of $\langle p_\perp \rangle$ with x is also observed in nonannihilation processes. However, in this case the effect is much weaker [the values of $\langle p_\perp \rangle$ reach ~ 0.4–0.5 GeV/c at $x \sim 0.5$ (Ref. 69)]. The "seagull" effect finds a natural explanation in the model of color strings. Indeed, the hadrons in the fragmentation regions of the initial particles are formed as a result of decays into sections of the V-shaped configuration of two triplet strings, and this leads to a growth of $\langle p_\perp \rangle$ with increasing x. The estimates made above for the contributions to σ_{ann}^{NN} from the mechanisms of Figs. 7a and 6c show that the probability of formation of hadrons in the N (or $\bar{N}$) fragmentation region as a result of decay of a configuration with a string junction in the N (or $\bar{N}$) fragmentation region (diagram of Fig. 8a) is small (about 20%). Therefore, as in the case of nonannihilation events, their production can, in a first approximation, be represented as a process of hadronization of a V-shaped configuration of triplet strings. At the same time, because of the higher transverse momenta of the ends of the strings in annihilation events compared with nonannihilation events, the dependence of $\langle p_\perp \rangle$ on x in the first case must be steeper. Calculations of the dependence of $\langle p_\perp \rangle$ on x in NN interactions were made in the framework of the MQGS in Ref. 8. A reasonable description of the experimental data was obtained. For the annihilation mechansims of Fig. 7, calculations of $\langle p_\perp(x) \rangle$ were made in Ref. 70. It was shown that the seagull effect in $\bar{p}p$ annihilation can be reproduced if a component of the nucleon wave function with a compact diquark is taken into account.

To conclude the discussion of the preasymptotic mechanisms of $\bar{p}p$ annihilation, we consider the ratio of the mean multiplicities in the annihilation and nonannihilation channels. It has been noted experimentally (at $E_{\text{lab}} \sim 10$ GeV) that the mean multiplicity in $\bar{p}p$ annihilation exceeds the mean multiplicity in pp interactions: $\langle n \rangle_{\text{ann}} / \langle n \rangle_{pp} \approx 1.5$. Usually, this is assumed (Refs. 1, 15, 16, and 20–22) to be an important argument for dominance of the annihilation mechanism with three-sheet topology (see Fig. 3c). However, we shall show that the experimentally observed ratio $\langle n \rangle_{\text{ann}} / \langle n \rangle_{pp}$ agrees better with the two-sheet annihilation mechanism.

We use the results of the fit in Ref. 5 to the data on e^+e^- annihilation and deep inelastic scattering for the mean multiplicities of the particles produced on hadronization of $\bar{q}q$ and Dq strings:

$$\langle n \rangle_{\bar{q}q} = 2.1 + 0.85 \ln(s/s_0),$$

$$\langle n \rangle_{Dq} = 0.8 + 0.9 \ln(s/s_0),$$

$$s_0 = 1 \text{ GeV}^2. \tag{70}$$

It can be seen that at low energies $\langle n \rangle_{\bar{q}q}$ appreciably exceeds $\langle n \rangle_{Dq}$. Using (70) for $E_{\text{lab}} \approx 10$ GeV, we can obtain in the case of the three-sheet annihilation mechanism $\langle n \rangle_{\text{ann}} / \langle n \rangle_{pp} \approx 1.9$ (with allowance for the fact that the cut of the Pomeron in pp scattering corresponds to two Dq strings). Thus, for the three-sheet annihilation mechanism a value of $\langle n \rangle_{\text{ann}} / \langle n \rangle_{pp}$ appreciably exceeding the one observed experimentally is predicted. In contrast, for the mechanisms of Fig. 8, for which the multiplicity must be close to the multiplicity of two $\bar{q}q$ strings, we obtain $\langle n \rangle_{\text{ann}} / \langle n \rangle_{pp} \approx 1.55$, in good agreement with experiment.

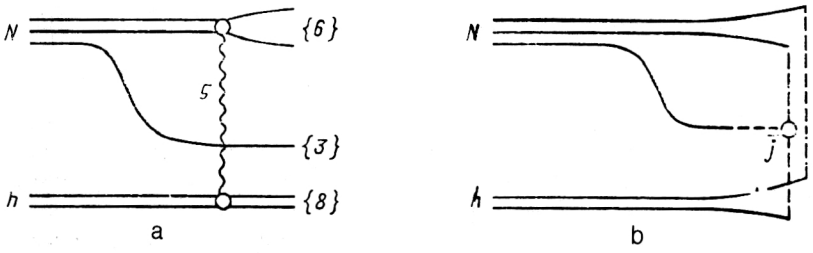

FIG. 17. Mechanism of baryon-number transfer to the central rapidity region associated with diquark disintegration and the presence of a slow valence quark in the nucleon wave function: a) perturbation-theory diagram for the first stage of the Nh interaction; b) string configuration formed in the nonperturbative stage of the Nh interaction.

4. TRANSFER OF BARYON NUMBER THROUGH A LARGE RAPIDITY INTERVAL

Derivation of a formula for the inclusive cross section of the process $ph \to pX$ in the central rapidity region

In estimates of the contribution to $\sigma_{\text{ann}}^{\bar{p}p}$ from the preasymptotic mechanisms of $\bar{p}p$ annihilation, appreciable uncertainties arise because of the errors in the estimates of the partial probabilities of decays of the configuration M_4^J into mesons (for the diagrams of Figs. 7a and 7b) and lack of knowledge of the color structure of the $\bar{q}q$ Reggeons and of the degree of violation of exchange degeneracy of the ω and f Reggeons (for the diagram of Fig. 7c). Therefore, the qualitative agreement between the total contribution of the mechanisms of Fig. 7 to the cross section of $\bar{p}p$ annihilation with the experimentally observed $\sigma_{\text{ann}}^{\bar{p}p}$ at $E_{\text{lab}} \sim 10$ GeV cannot yet be regarded as a convincing confirmation of the correctness of the estimates of the cross sections for the formation of string configurations with diquarks in color sextet states. To test the proposed scheme of generation of the new string configurations, it is very appropriate to compare the calculated and experimental inclusive cross sections of processes of the type $ph \to pX$ with transfer of the proton to the central rapidity region.

In our approach, there exists a mechanism of proton transfer to the central region of rapidities in ph collisions; in its nature, it is close to the preasymptotic annihilation mechanisms associated with Pomeron cutting. This mechanism can be described by the diagram of Fig. 17a, which shows a process with a transition $D_{\{\bar{3}\}} \to D_{\{6\}}$ as a result of exchange of a gluon between the diquark and the hadron h under the condition that the valence quark in the wave function of the ph system is in the central region of rapidities. This mechanism leads to the formation of the string configuration shown in Fig. 17b. Its decay is accompanied by the production of a baryon in the central rapidity region. Indeed, if the slow valence quark in the diagram of Fig. 17a is situated in the rapidity space at an appreciable distance from the fragmentation regions of the initial particles, then the rapidity of the proton produced on hadronization of the string configuration of Fig. 17b can be identified with the quark rapidity. Then the inclusive cross section of the process $ph \to pX$ in the central region of rapidities associated with the mechanism of Fig. 17a can be expressed in the form

$$\frac{d\sigma}{dy}(ph \to pX) \approx K\tilde{\sigma}_{\{6\}} W_q(y). \tag{71}$$

Here, K is the spin–isospin factor; $W_q(y)$ is the rapidity distribution for the valence quark in the wave function of the ph system; $\tilde{\sigma}_{\{6\}}$ is the cross section of the process $D_{\{\bar{3}\}}h \to D_{\{6\}}h_{\{8\}}$. Note that the calculation of $\tilde{\sigma}_{\{6\}}$ must take into account all octet states of the hadron h. Therefore, for $h = N$, the cross section $\tilde{\sigma}_{\{6\}}$ is not equal to the cross section $\sigma_{\{6\}}$ in (27), in the calculation of which the nucleon was regarded as a $qD_{\{3\}}$ system in the initial and final states. A simple calculation using (29) and (30) leads to the following expression for $\tilde{\sigma}_{\{6\}}$:

$$\tilde{\sigma}_{\{6\}} = \frac{4\pi\alpha_s^2 n_h}{3} \int_0^\infty \frac{d\mathbf{q}^2}{(\mathbf{q}^2 + M_g^2)^2} \times [1 - F_D(\mathbf{q})][1 - F_h(\mathbf{q})], \tag{72}$$

where

$$F_h(\mathbf{q}) = \langle h \,|\exp[i\mathbf{q}(\mathbf{r}_1 - \mathbf{r}_2)]\,|h\rangle$$

is the two-quark form factor of the hadron h. The expression (72), like the expressions for $\sigma_{\{6\}}$ and $\sigma_{\{6,6\}}$, is infrared-stable. Therefore, to estimate $\tilde{\sigma}_{\{6\}}$ we can set $M_g = 0$ in (72). Normalizing α_s in (72) by the same procedure as in Secs. 2 and 3, we can obtain from the expression (72) the following results for variants I and II of the model nucleon wave function:

$$\sigma_{\{6\}}(h=p,\bar{p}) = \begin{cases} 15 \cdot 10^{-27}\ \text{cm}^2\ \text{(I)}, \\ 11 \cdot 10^{-27}\ \text{cm}^2\ \text{(II)}. \end{cases} \tag{73}$$

The value of $W_q(y)$ is determined by the expression (40). However, to analyze the data on the process $ph \to pX$, we shall calculate the normalization factor C in (40), not by means of (39), but by means of a more accurate formula that takes into account the influence of the additional $\bar{q}q$ pairs in the wave function of the ph system:[6,7]

$$C_{\text{eff}} = \sum_{n=1}^{\infty} C_n \frac{\sigma_{\text{in}}^n}{\sigma_{\text{in}}}. \tag{74}$$

Here, σ_{in}^n is the contribution to σ_{in} associated with the cutting of n Pomerons, and, following Refs. 6 and 7, we shall calculate it in the eikonal model; C_n is the normalization factor in the formula for the distribution of the valence quarks in the presence of $n-1$ additional $\bar{q}q$ pairs in the nucleon wave function. The formula for C_n is obtained from (39) by the substitution $\beta \to \beta - n + 1$ (Refs. 6 and 7). At ISR energies, Eq. (74) leads to an increase of C_{eff} compared with the prediction of (39) by about 15%. Note that for our method of determining $W_q(y)$ this factor in (71) can be regarded as effectively extracted from the

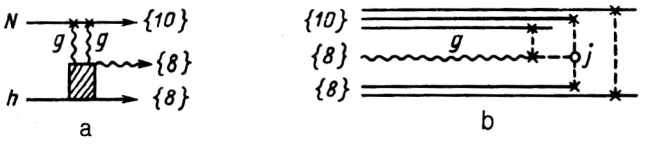

FIG. 18. Mechanism of baryon-number transfer to the central rapidity region associated with color decuplet exchange: a) perturbation-theory diagram for the perturbative stage of the *Nh* interaction; b) string configuration formed in the nonperturbative stage of the *Nh* interaction process for the mechanism of Fig. 18a.

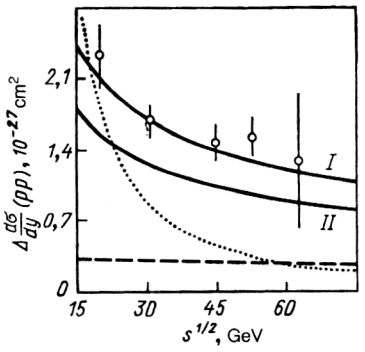

FIG. 19. Difference between the p and $\bar{p}$ production cross sections for $y=0$ in pp collisions at ISR energies.[71] Curves I and II correspond to the expression (75); the dotted line shows the contribution from fragmentation of the diquark[73] into a proton; the broken line gives the contribution associated with the difference between the probabilities of quark fragmentation into p and $\bar{p}$.

experimental data. Indeed, in the MQGS the growth of the inclusive spectra in the central region of rapidities associated with diagrams involving an undeveloped cylinder is strictly related to the probability of finding a valence quark in the central rapidity region. At the same time, calculations show that in our approach to the determination of $W_q(y)$ the growth of the inclusive spectra at $y\approx 0$ for $\bar{p}p$ and pp collisions is reproduced well.

We shall estimate the spin–isospin factor K in (71) under the following simplifying assumptions:

a) only the formation of $SU(3)_F$ octet and decuplet states of the baryons need be taken into account on the hadronization of the string configuration of Fig. 17b;

b) the probability of production of $\bar{s}s$ pairs is suppressed by a factor 1/3 compared with the probability of the production of nonstrange $\bar{q}q$ pairs;

c) the ratio of the distribution functions of the valence u and d quarks in the proton wave function is equal to 2.

Under these assumptions, we obtain $K\approx 0.5$.

The final expression for the contribution of the mechanism of Fig. 17a to the inclusive cross section of the process $ph\to pX$ at $y\sim 0$ for $h=p,\bar{p}$ has the form

$$\frac{d\sigma}{dy}(ph\to pX) \simeq \left(\sqrt{\frac{s_0}{s}}\right)^{1-\alpha_R(0)} \{\exp[y(1-\alpha_R(0))]+\varepsilon \times \exp[-y(1-\alpha_R(0))]\} \begin{cases} 4.7\cdot 10^{-27}\ \text{cm}^2\ \text{(I)}, \\ 3.5\cdot 10^{-27}\ \text{cm}^2\ \text{(II)}, \end{cases} \tag{75}$$

where

$$\varepsilon=\begin{cases} 0, & h=\bar{p} \\ 1, & h=p, \end{cases} \quad s_0=1\ \text{GeV}^2.$$

The expression for the inclusive cross section of the process $p\bar{p}\to\bar{p}X$ is obtained from (75) by the substitution $y\to -y$ (we assume that for the initial proton $y>0$).

Besides the considered mechanism of transfer of baryons to the central rapidity region, the nature of which is intimately related to the preasymptotic annihilation mechanisms, there exists another mechanism of transfer of baryons through a large rapidity interval; like the asymptotic mechanism of $\overline{B}B$ annihilation, it is related to exchange of a pair of gluons in the color {10} state. This mechanism is described by diagrams like that of Fig. 18a. Separation of the quarks and gluons corresponding to the final state of the perturbation-theory diagrams of the form shown in Fig. 18a in the nonperturbative stage of the process must lead to formation of the string configuration of Fig. 18b. Its hadronization is accompanied by the appearance of a baryon in the central rapidity region. The estimates of the contribution of the mechanism of Fig. 18a to $(\partial\sigma/dy)(pp\to pX)$ made in Ref. 41 give a value that does not exceed $\sim 0.1\times 10^{-27}$ cm^2. For ISR energies, the cross section predicted by (75) exceeds this value by a factor $\sim$10–20. Therefore, in analyzing the ISR data below we shall not take into account the mechanism of Fig. 18a.

Transfer of protons through a large rapidity interval in *ph* collisions. Comparison with experiment

The expression (75) does not take into account the contribution to the cross section of the process $ph\to pX$ from protons produced as a result of the production of sea $p\overline{B}$ pairs in the central rapidity region. Therefore, the predictions of (75) should be compared, not with the experimentally observed cross section $(\partial\sigma/dy)(ph\to pX)$, but with the difference between the experimental cross sections of the processes $ph\to pX$ and $ph\to\bar{p}X$. In Fig. 19, we give the points for $\Delta(d\sigma/dy)(pp)=(d\sigma/dy)(pp\to pX)-(d\sigma/dy)(pp\to\bar{p}X)$ at $y=0$ obtained from ISR data.[71] The predictions of Eq. (75) for the variants I and II of the nucleon wave function, and also the predictions in Fig. 19, agree well with the experimental data. This is also indicated by the fit to the data by means of the parametrization $\Delta(d\sigma/dy)(pp)|_{y=0}=b(s/1\ \text{GeV}^2)^{-\beta/2}$, which gives $b=(8.7\pm 6.4)\times 10^{-27}$ cm^2 and $\beta=0.46\pm 0.21$. These values are close to the ones expected for the mechanism of Fig. 17a [see Eq. (75)].

It is also of interest to verify the y dependence of the proton-transfer cross section predicted by (75). In the study of Ref. 72, the inclusive cross sections for the production of protons and antiprotons in $\bar{p}p$ and pp interactions in the interval $-0.4<y<0.4$ were measured. The results were represented in the form of the ratio

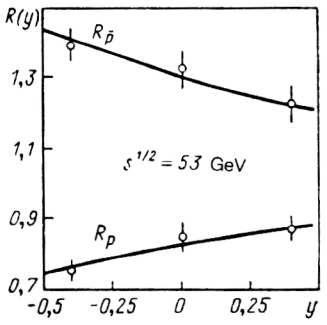

FIG. 20. Data of Ref. 72 for the ratio $R_{p(\bar{p})}(y)$ defined in (76). The curves show the results of a fit by means of the expression (77) for the parameter values (78).

$$R_{p(\bar{p})}=\frac{d\sigma(p\bar{p}\to p(\bar{p})X)/dy}{d\sigma(pp\to p(\bar{p})X)/dy}. \tag{76}$$

To verify the dependence on y predicted in (75), we analyze the data of Ref. 72 as follows. In (76) we parametrize the inclusive cross sections in the form (we assume that the rapidity of the initial proton is greater than zero)

$$\frac{d\sigma}{dy}(p\bar{p}\to\bar{p}X)=\delta\alpha+\beta e^{-\tau y};$$

$$\frac{d\sigma}{dy}(pp\to\bar{p}X)=\alpha;$$

$$\frac{d\sigma}{dy}(p\bar{p}\to pX)=\delta\alpha+\beta e^{\tau y};$$

$$\frac{d\sigma}{dy}(pp\to pX)=\alpha+\beta(e^{\tau y}+e^{-\tau y}). \tag{77}$$

Here, the first terms correspond to sea protons and antiprotons. The factor δ is introduced to take into account the possible difference between the cross sections for production of sea particles in $\bar{p}p$ and pp collisions. The final terms in (77) correspond to transferred protons and antiprotons. Fitting of the free parameters in (77) by comparison with the values of $R_{p,\bar{p}}$ obtained in Ref. 72 gives

$$\tau=0.76\pm0.22;\quad \delta=1.01\pm0.02;$$

$$\beta/\alpha=0.3\pm0.03. \tag{78}$$

The factors $R_{p,\bar{p}}$, calculated with these values of the parameters and obtained from the experimental cross sections in Ref. 72, are given in Fig. 20. It can be seen that the functional dependence on y is well reproduced. It is important that at the same time, to within the errors, the value of τ agreed with the value expected from (75): $\tau = 1 - \alpha_R(0) \approx 0.57$ [we assume $\alpha_R(0) = \alpha_\omega(0)$]. To within the errors, the value of the parameter δ also agrees with the ratio of the inclusive cross sections of the charged particles in the $\bar{p}p$ and pp interactions.

Thus, the experimental data of Refs. 71 and 72 agree well with the proton-transfer mechanism associated with the diagram of Fig. 17a. At the same time, the behavior of $\Delta(d\sigma/dy)(pp)$ observed in Ref. 71 could not be described in the standard MQGS without allowance for the transition $D_{\{\bar{3}\}} \to D_{\{6\}}$. Calculations of the proton spectra in this form of the MQGS were made in Ref. 73, where, however, a comparison with the data of Ref. 71 was not made. In the absence of $D_{\{\bar{3}\}} \to D_{\{6\}}$ transitions, the difference of $\Delta(d\sigma/dy)(pp)|_{y=0}$ from zero is due to difference of the fragmentation functions $D_D^p(z)$ from $D_D^{\bar{p}}(z)$ and $D_q^p(z)$ from $D_q^{\bar{p}}(z)$. Figure 19 gives the contributions of these two mechanisms to $\Delta(d\sigma/dy)(pp)|_{y=0}$, calculated with the fragmentation functions from Ref. 73 (it is assumed that there are no $D_{\{\bar{3}\}} \to D_{\{6\}}$ transitions). We do not describe the technique of the calculations, since it is explained in Ref. 73. We merely mention that since we are concerned with the region $y \sim 0$, we did, in contrast to Ref. 73, take into account transfer of protons from both initial protons in the case of pp collisions. As can be seen from Fig. 19, the contribution of the mechanism associated with diquark fragmentation decreases rapidly with the energy ($\sim s^{-1}$). The contribution of the mechanism associated with quark fragmentation decreases slowly with the energy (in the asymptotic region, as $s^{-1/4}$), but its absolute value is much smaller. Thus, in the standard MQGS it is not possible to describe the data of Ref. 71.

It should be said that in the approach that takes into account $D_{\{\bar{3}\}} \to D_{\{6\}}$ transitions it is also necessary to take into account contributions to $\Delta(d\sigma/dy)(pp)|_{y=0}$ that are not associated with diquark disintegration. The calculations of $\tilde{\sigma}_{\{6\}}$ made above indicate that the probability of absence of $D_{\{\bar{3}\}} \to D_{\{6\}}$ transitions in the collision process is $\sim$0.5–0.6. Therefore, to the contribution of the mechanism of Fig. 17 to $\Delta(d\sigma/dy)(pp)|_{y=0}$ it is necessary to add approximately half of $\Delta(d\sigma/dy)(pp)|_{y=0}$ calculated in the MQGS without $D_{\{\bar{3}\}} \to D_{\{6\}}$ transitions. With allowance for this addition, variant II of the nucleon wave function gives somewhat better agreement with experiment. The part played by the processes without diquark disintegration becomes negligibly small for $\sqrt{s} \gtrsim 30$ GeV. However, we assume that addition of the contribution of the mechanism of Fig. 17 to the contribution of the mechanisms without diquark disintegration, calculated with the fragmentation functions from Ref. 73, is hardly meaningful. The fact is that in the standard form of the MQGS one must evidently choose a diquark-to-proton fragmentation function that is too soft to imitate the effects associated with the $D_{\{\bar{3}\}} \to D_{\{6\}}$ transitions. Therefore, in reality the contribution of the mechanisms without diquark disintegration to $\Delta(d\sigma/dy)(pp)|_{y=0}$ at ISR energies can be much smaller than is shown in Fig. 19.

One further argument for a connection between the processes with proton transfer through a large rapidity interval and diquark disintegration is the experimentally observed[74,75] difference between the cross sections for the processes $\pi^+ p \to pX$ and $\pi^- p \to \bar{p}X$ in the pion fragmentation region. The impossibility of describing this phenomenon in the standard form of the MQGS was pointed out in Ref. 76. In our approach, this effect can be related to a diagram like that of Fig. 17a, provided that a valence quark is transferred to the pion fragmentation region. Naturally, at the same time there are no longer any

grounds for using Eq. (71). However, it is clear that this mechanism must lead to a decrease with the energy of the difference $\Delta(d\sigma/dx)(\pi p) = (d\sigma/dx)(\pi^+ p \to pX) - (d\sigma/dx)(\pi^- p \to \bar{p}X)$ for fixed X in accordance with the law $\sim s^{-1/2}$. Fitting of $\Delta(d\sigma/dx)(\pi p)|_{x=0.5}$ in accordance with the data of Refs. 74 and 75 by a dependence $\sim s^{-\beta}$ gives $\beta = 0.56 \pm 0.11$, in good agreement with a mechanism like that of Fig. 17a.

Diquark disintegration and inclusive cross sections in the nucleon fragmentation region

The estimates given above for the $D_{\{3\}}h \to D_{\{6\}}h_{\{8\}}$ cross sections indicate that in 40–50% of all inelastic events in ph interactions there is a transition of a diquark from an antitriplet to a sextet color state. In this connection, it becomes clear that the picture adopted in the standard MQGS for hadron production in the proton fragmentation region in the form of fragmentation of a diquark (in a color $\{\bar{3}\}$ state) and a quark does not correspond to reality. The following natural question arises: How can one explain in the standard MQGS the spectra of the particles in the proton fragmentation region (see, for example, Refs. 6–8, 73, and 76)? It appears to us that this is simply related to the existing arbitrariness in the choice of the diquark fragmentation functions, on which the spectra of the secondary particles in the region of X not too near zero basically depend. For example, in the approach that determines the diquark fragmentation functions by means of the cascade equations of Ref. 77 there is an arbitrariness in the choice of the kernels of these equations. In Kaĭdalov's method,[4,78] the fragmentation functions $D_D^B(z)$ and $D_D^M(z)$ are chosen on the basis of a smooth extrapolation between the two Regge asymptotic regimes $z \to 0$ and $z \to 1$. At the same time, sum rules for the momentum and baryon number are taken into account. However, in this scheme one can always choose a different smooth extrapolation without violating the sum rules. Thus, neither method can answer the question of how the probability of finding a proton in the case of diquark fragmentation decreases with z (we do not now discuss sea $\bar{B}B$ pairs produced in the central rapidity region). As a result, the main criterion for choosing the functions of diquark fragmentation into baryons and mesons is the possibility of describing the experimental spectra.

At the same time, the need to imitate the effects associated with the $D_{\{\bar{3}\}} \to D_{\{6\}}$ transitions forces one to take the diquark–baryon fragmentation functions softer but the diquark–meson fragmentation functions harder. Indeed, because the slow valence quark carries on the average about 10% of the nucleon momentum,[4] which is not taken into account in the standard MQGS, the mechanism of Fig. 7 leads mainly to the production of soft baryons. Therefore, when allowance is made in the MQGS for $D_{\{\bar{3}\}} \to D_{\{6\}}$ transitions there is obviously no need to transfer the baryon number to the soft region of the spectrum by choosing fragmentation functions $D_D^B(z)$ that decrease slowly as $z \to 0$. In contrast, in the case of the meson spectra the mechanism of Fig. 17 is an effective means of production of hard mesons, and this makes it possible to use softer diquark-to-meson fragmentation functions. Unfortunately, the absence of a theory of hadronization of string configurations with a string junction makes it impossible to carry out a systematic analysis of the experimental data on the spectra of the secondary particles in the proton fragmentation region in the approach that takes into account diquark disintegration.

Nevertheless, we did attempt to estimate qualitatively the influence of the diagram of Fig. 17 on the meson spectra in the region $x \gtrsim 0.5$, since the following question may arise: Could not allowance for the diagram of Fig. 17 lead to a manifest contradiction with the data on the meson spectra in the hard region? Bearing in mind that the quark carries about 10% of the nucleon momentum, the meson spectra in the hard part ($x \gtrsim 0.5$) for the string configuration of Fig. 17b can be calculated approximately by considering the fragmentation of two quarks. We parametrized the distribution function of the quarks in the diquark in the form

$$f_{q/D}(x) = Ax^n(1-x)^n. \tag{79}$$

To calculate the meson spectra, we took the distribution function of the diquarks in the nucleon and the quark-to-meson fragmentation functions to be the same as in Refs. 6–8. Comparison of the calculated pion spectra (processes without $D_{\{\bar{3}\}} \to D_{\{6\}}$ transitions were also taken into account) with the data of Ref. 74 shows that a contradiction with the experimental pion spectra in the hard region does not arise if in (79) we set $n \approx 2.5$. For this value of n and $1 - x \gtrsim 0.05$, the distribution (79) agrees to accuracy $\sim$20–30% with the x distribution of the quarks in the diquark for a relativistic two-particle wave function of the form

$$\Psi_D(x, p_\perp) \sim \frac{1}{\sqrt{x(1-x)}} \exp\left[-\frac{\alpha(m_q^2 + p_\perp^2)}{x(1-x)}\right] \tag{80}$$

with parameters $m_q = 0.27$ GeV/c^2 and $\alpha \simeq 1.5$–2 GeV^{-2}. Calculation of the diquark form factor with the wave function (80) shows that for these values of m_q and α the diquark radius is about 0.4–0.5 F. This value appears reasonable in the light of the existing indications of the presence, in the nucleon wave function, of a component with a compact diquark.[48–54] Thus, allowance for the $D_{\{\bar{3}\}} \to D_{\{6\}}$ transitions in the MQGS does not lead to a contradiction with the experimental data on the pion spectra.

$D_{\{\bar{3}\}} \to D_{\{6\}}$ transitions in pA collisions

Processes with transitions of diquarks from triplet to sextet color states can be even more important in the case of collisions of protons with nuclei. Indeed, for a sufficiently thick nucleus the sequence of color charge exchanges must have the consequence that both quarks in the diquark go over to a state that is unpolarized in the color space. Then the ratio of the probabilities of finding the diquark in the color $\{\bar{3}\}$ and $\{6\}$ states will be 1:2. The increase in the probability of the $D_{\{\bar{3}\}} \to D_{\{6\}}$ transition for nuclear targets compared with a proton target must have the consequence that the proton spectra in the $pA \to pX$

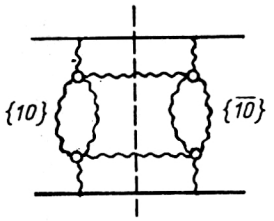

FIG. 21. Inclusion of decuplet color exchanges in the QCD perturbative Pomeron.

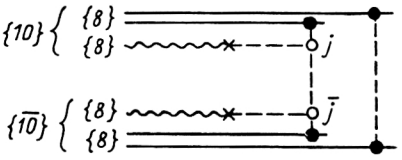

FIG. 22. String configuration formed in the nonperturbative stage of the hadron interaction corresponding to the perturbation-theory diagram in Fig. 21.

processes will be shifted to the soft region of the spectrum compared with the $pp \to pX$ process. The effect of the softening of the proton spectra in the case of nuclear targets (nuclear stopping power) was indeed observed in the experiment of Ref. 79. It has been intensively discussed in the literature.[79–83] However, the importance of taking into account $D_{\{\bar{3}\}} \to D_{\{6\}}$ transitions has not hitherto been considered. The strong "stopping" of the protons in pA interactions is sometimes[79,83] regarded as an indication of the possible appearance of large specific energy densities in the nuclear target, which could lead to the formation of a phase of a quark–gluon plasma. However, if the softening of the proton spectra in pA collisions compared with pN collisions is due to $D_{\{\bar{3}\}} \to D_{\{6\}}$ transitions, then there is no loss of energy of the quarks that form the proton (we do not take into account the loss associated with the tension of the strings that are formed; for times of the order of the collision time it can be ignored). In this case, there is "stopping" of only the baryon number, and not of the proton as a whole.

New mechanism of $\bar{B}B$ pair production in the central rapidity region

We have seen above that in reactions with baryon transfer through a large rapidity interval not only the mechanism of Fig. 17a but also the mechanism associated with exchange of a pair of gluons in a color {10} state (see Fig. 18a) can play a part. It turns out that decuplet exchange also leads to a distinctive mechanism of production of sea $\bar{B}B$ pairs in the central rapidity region with transfer of baryon number through a large rapidity interval. This effect is associated with inclusion, in the ladder diagram of the perturbative Pomeron,[66] of exchanges of a pair of gluons in the color {10} state (Fig. 21). The perturbation-theory state corresponding to the cut of the diagram of Fig. 21 must lead, in the nonperturbative stage of the hadron interaction process, to the formation, in the vacuum, of the string configuration shown in Fig. 22. Its hadronization will be accompanied by production, in the central rapidity region, of a pair of a baryon and an antibaryon whose rapidities will be close to those of the s-channel gluons in the graph of Fig. 21. The mechanism of $\bar{B}B$ pair production by tunnel production from the vacuum of $\bar{D}D$ pairs, which is usually considered in the MQGS, leads to production of a baryon and an antibaryon separated by a small rapidity interval. In contrast to this mechanism, hadronization of the string configuration of Fig. 22 can lead to production of a baryon and an antibaryon with a large relative separation on the rapidity scale. This property could be the signature of the mechanism of $\bar{B}B$ pair production associated with exchange of a pair of gluons in the color decuplet state.

5. LOW ENERGIES

Unitarization of the elastic $\bar{p}p$ scattering amplitude

One of the puzzling phenomena observed in $\bar{p}p$ interactions at low energies (hundreds of mega-electron-volts) is the strong growth of the interaction range. Whereas in elastic pp scattering at these energies the S wave is dominant, a rather large number of waves contribute to $\bar{p}p$ scattering, and the slope parameter reaches huge values ~ 40 $(\text{GeV}/c)^2$. This effect cannot be explained by any nearby t-channel singularities.

With decreasing initial energy of the $\bar{p}p$ collision, the interaction cross section (due mainly to the annihilation channels) increases so much that unitarity corrections become important. We shall consider the consequence of this for the example of hadron interactions at superhigh energies, where there is a similar situation, although the growth of the cross section has other causes.

The growth of the hadron interaction cross sections at high energies is most simply described in Regge phenomenology by introduction of a Pomeranchuk pole in the j plane to the right of unity.[84] Calculations in QCD perturbation theory[66] do indeed show that the vacuum singularity (which is more complicated than a simple pole[65]) is to the right of unity. At the same time, the partial-wave amplitude

$$f(\mathbf{b}) = f(0)\exp(-\mathbf{b}^2/2B) \tag{81}$$

($\mathbf{b}$ is the impact parameter) increases with the energy, violating unitarity, since

$$f(0) = i a \nu^{\Delta}. \tag{82}$$

Here, $\nu = 2m_N E/s_0$, E is the initial energy in the laboratory system, $s_0 = 1$ GeV^2, and $\Delta = \alpha_{\mathbf{P}}(0) - 1$ is the amount by which the Pomeron intercept exceeds unity.

The simplest way to unitarize the amplitude is to sum the graphs with different numbers of Pomerons in the eikonal approximation.[84]

The scattering amplitude takes the form

$$F(\mathbf{b}) = i\{1 - \exp[i f(\mathbf{b})]\}. \tag{83}$$

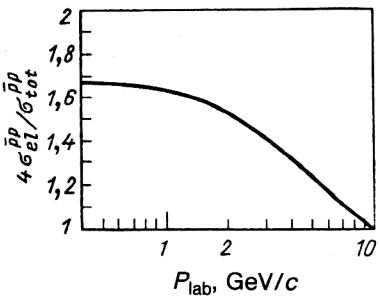

FIG. 23. Result of calculation of $h\sigma_{el}^{\bar{p}p}/\sigma_{tot}^{\bar{p}p}$ from experimental data for $\bar{p}p$ collisions.[58]

It is readily seen that substitution of (81) in (83) leads to a slope that increases rapidly at asymptotic energies:

$$B_{\text{eff}}=\tfrac{1}{2}B\Delta \ln \nu.$$

At the same time, the "bare" slope B need not depend on the energy at all. For $f(0)\gg 1$, the amplitude (83) corresponds to scattering by a "black" disk with radius $R^2=2B\Delta \ln \nu$.

It turns out that a similar picture holds in $\bar{p}p$ scattering at low energies.[37] To a high accuracy, the scattering amplitude is imaginary. With decreasing energy, the increasing contribution of ω exchange and of the annihilation channels leads to violation of unitarity in the amplitude (81). As a result, the **b** dependence of the amplitude (83) becomes essentially non-Gaussian. Indeed, for an amplitude having a Gaussian form we can readily show that

$$\operatorname{Im} f(0)=4\sigma_{\text{el}}/\sigma_{\text{tot}}. \tag{84}$$

The results of substitution of the experimental data of Ref. 58 in the right-hand side of (84) are shown in Fig. 23. It can be seen that at momentum $P_{\text{lab}} < 10$ GeV/c the Gaussian form of the partial-wave amplitude (81) contradicts unitarity. However, if the amplitude (81) is unitarized by the method (83), then the total interaction cross section takes the form

$$\sigma_{\text{tot}}=4\pi B\{\gamma+\ln[\operatorname{Im} f(0)]-\operatorname{Ei}[-\operatorname{Im} f(0)]\}. \tag{85}$$

Here, $\gamma=0.5772$ is Euler's constant, and $\operatorname{Ei}(-z)$ is the exponential integral.

We first fit the experimental data of Ref. 58 on the total cross sections $\sigma_{\text{tot}}^{\bar{p}p}$ at high energies $p_{\text{lab}} > 10$ GeV/c, where the $\bar{p}p$ scattering amplitude is determined by the contributions of Pomeron exchange (82) and of exchange of secondary Reggeons ω, f, ρ, A_2,

$$\operatorname{Im} f_R(0)=b/\sqrt{\nu}, \tag{86}$$

and also by the annihilation graphs of Fig. 9c, which have the same energy dependence as (86).

For the fit, we shall for simplicity assume that these contributions to (81) have the same dependence on b^2 as the slope parameter:

$$B=B_0+2\alpha'_{\text{P}} \ln \nu. \tag{87}$$

The value of B_0 is determined by the nucleon form factor and can be related to the mean-square radius: $B_0=2\langle r_N^2\rangle/3\approx 10.8$ GeV^{-2}. At the same time, the fit to the data on the slope of the differential cross section for pp scattering[65] leads to $B_0=8.9$–10.15 GeV^{-2}. We took $B_0=10$ GeV^{-2}. The parameters Δ and α'_{P} were also fitted.[65] The corresponding values, and also the results of the fit for the parameters a and b, are given in Table II.

At lower energies, the annihilation associated with the planar graph of Fig. 3a becomes important. The energy dependence of its contribution to the total cross section is determined by a Regge trajectory on which diquark–antidiquark ($D\bar{D}$) bound states lie. The intercept of the trajectory is given by Eq. (1). We write the corresponding contribution to the amplitude in the form

$$\operatorname{Im} f_{D\bar{D}}(0)=c\nu^{2\alpha_N(0)-\alpha_R(0)-1}. \tag{88}$$

This contribution can be well determined in the range of momenta from 1 to 10 GeV/c. The use of the Regge dependence at such low energies is fully justified for this graph. For the Green's function for the $\bar{q}q$ system in the intermediate state the total c.m.s. energy, which in the given case is large even at the threshold, is important.

At momentum below 1 GeV/c, the annihilation mechanism associated with recombination of valence quarks, which is evidently dominant at the threshold,[85] becomes important. We parametrize this contribution in the form

$$\operatorname{Im} f_{\text{rec}}(0)=d/k^e, \tag{89}$$

where $k=(Em_N/2-m_N^2)^{1/2}$ is the momentum in the center-of-mass system of the $\bar{p}p$ collision. The values of the parameters c, d, e found from fitting the data are given in Table II.

In Fig. 24, the calculated curve is compared with the experimental data.[56,86] Also shown is the behavior of the curves without allowance for the contributions f_{rec} and

TABLE II. Values of the parameters that determine the bare $\bar{p}p$ scattering amplitude.

Δ	α'_{P}, GeV^{-2}	B_0, GeV^{-2}	a	b	c	d	e	h	g
0,1 *	0,13 *	10 *	0,39 ±0,001	3,71 ±0,03	23,73 ±0,05	0,0046 ±0,0002	2,68 ±0,02	1,95 ±0,05	0,75 ±0,03

Note. The asterisk identifies fixed parameters.

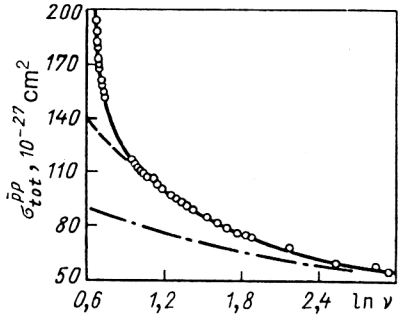

FIG. 24. Total cross section for $\bar{p}p$ scattering. The continuous curve is the result of the fit; the chain curve is for $c = d = 0$, and the broken curve for $d = 0$. The experimental points are from Refs. 58 and 86.

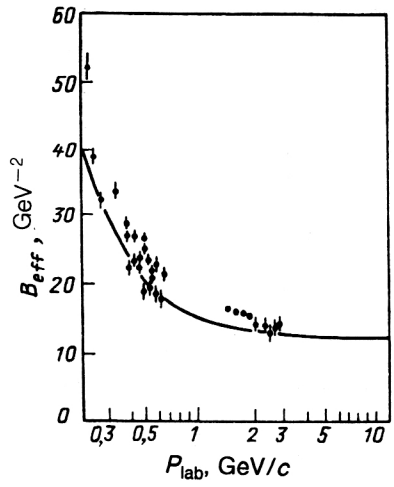

FIG. 26. Slope parameter of $\bar{p}p$ scattering. The data are from Refs. 87–90. The curve shows the calculation with the parameters from Table II.

$f_{\bar{D}D}$. It can be seen that the contribution (89) is important only when $p_{\text{lab}} \leqslant 1$ GeV.

It is important that the energy dependence of $\sigma_{\text{tot}}^{\bar{p}p}$ in the interval 1–10 GeV, fixed by the contribution (88), was found to be correct. This indicates that in this region diquark exchange is important.

Consequences of unitarization

Since it is known experimentally (see below) that the real part of the $\bar{p}p$ scattering amplitude is small, the cross section $\sigma_{\text{el}}^{\bar{p}p}$ can be expressed in terms of Im F:

$$\sigma_{\text{el}}^{\bar{p}p} = \int d^2\mathbf{b}\,|F(\mathbf{b})|^2$$
$$= 2\pi B\{\gamma + \ln[\operatorname{Im} f(0)/2] + \operatorname{Ei}[-2\operatorname{Im} f(0)]$$
$$- 2\operatorname{Ei}[-\operatorname{Im} f(0)]\}. \qquad (90)$$

The results of the calculation of $\sigma_{\text{el}}^{\bar{p}p}$ with the parameters fixed above are compared in Fig. 25 with the experimental data.[58] The agreement is an important confirmation of the correctness of the chosen dependence (83) of the partial-wave amplitude on $\mathbf{b}$. The possibility of calculating $\sigma_{\text{el}}^{\bar{p}p}$ at low energies knowing only $\sigma_{\text{tot}}^{\bar{p}p}$ is nontrivial. For example, if the form of the amplitude $F(\mathbf{b})$ is assumed to be Gaussian, then to calculate σ_{el} it is also necessary to know the slope parameter, which at low energies in $\bar{p}p$ scattering is large and appreciably greater than the nucleon diameter (see below). Here, we use only the known slope parameter of the "bare" amplitude $f(\mathbf{b})$; $B_0 \approx 10$ GeV^{-2}.

The effective slope parameter $B_{\text{eff}} = d\ln(d\sigma_{\text{el}}/d\mathbf{q}^2)/d\mathbf{q}^2|_{\mathbf{q}^2=0}$ for the amplitude (83) has the form

$$B_{\text{eff}} = \frac{1}{2}\langle \mathbf{b}^2 \rangle$$
$$= \frac{8\pi B^2}{\sigma_{\text{tot}}^{\bar{p}p}} \int_0^{\operatorname{Im} f(0)} \frac{dx}{x}\,[\gamma + \ln x - \operatorname{Ei}(-x)].$$

As can be seen from Fig. 26, the results of the calculation are in good agreement with the experimental data.[87–90] Thus, the long range of the $\bar{p}p$ interaction at low energies is a consequence of unitarization of the annihilation amplitude, i.e., mutual screening of processes with a large cross section.

The slope parameter characterizes only the mean-square interaction range. Direct comparison of the calculations with data on the differential cross section of elastic $\bar{p}p$ scattering is a more serious test of the present approach.

Knowing the partial-wave amplitude (83), we can readily calculate

$$\frac{d\sigma}{d\Omega_{\text{c.m.s.}}} = B^2k^2 \left| \int_0^{\operatorname{Im} f(0)} \frac{dx}{x}\,(1 - e^{-x}) J_0(qb) \right|^2. \qquad (91)$$

Here, k is the momentum in the $\bar{p}p$ center-of-mass system, $J_0(z)$ is a Bessel function, $q^2 = 2k^2(1 - \cos\theta)$, and $b = 2B\ln[\operatorname{Im} f(0)/x]$.

The results of the calculation of $d\sigma/d\Omega$ are compared in Fig. 27 with the data of Ref. 91. It is remarkable that formulas valid only in the region of diffraction scattering describe the data right up to angles $\sim 90°$ so well.

We now consider the contribution of the terms (82), (86), (88), and (89) to the real part of the $\bar{p}p$ forward scattering amplitude. The contribution of the first two

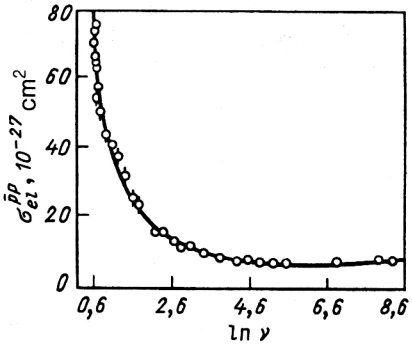

FIG. 25. Total cross section for elastic $\bar{p}p$ scattering. The data are from the compilation of Ref. 58. The curve is the result of a calculation with the parameters from Table II.

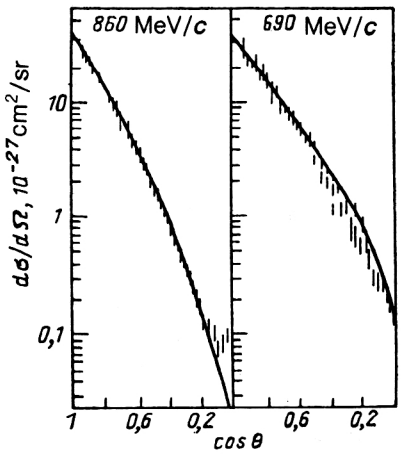

FIG. 27. Differential cross sections for elastic $\bar{p}p$ scattering. The data are from Ref. 91. The curve is the result of calculation with the parameters from Table II.

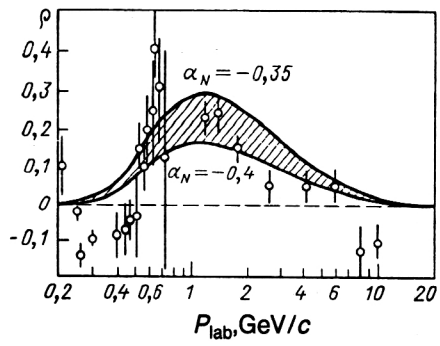

FIG. 28. Ratio of the real to the imaginary part of the $\bar{p}p$ forward scattering amplitude. The data are taken from Refs. 87–89 and 92. The curve is the calculation with the parameters from Table II.

terms is small, for the Pomeron because the intercept is near unity, and for the secondary Reggeons because of the cancellations in the real part due to the ω–f and ρ–A_2 exchange degeneracy. The contribution of the trajectories (88) does not cancel in the real part. Indeed, the ratio $\rho_{D\bar{D}} = \mathrm{Re}\, f_{D\bar{D}}(q)/\mathrm{Im}\, f_{D\bar{D}}(q)\,|_{q=0}$, which is determined by the signature factors, is

$$\rho_{D\bar{D}}=\frac{1}{2}\left[\tan\frac{\pi\alpha_{D\bar{D}}(0)}{2}-\cot\frac{\pi\alpha_{D\bar{D}}(0)}{2}\right]. \qquad (92)$$

As we have already said, $\alpha_{D\bar{D}}(0) = 2\alpha_N(0) - \alpha_R(0) = -1.3$ if $\alpha_N(0) = -0.4$ (from the baryon mass spectrum). Accordingly, $\rho_{D\bar{D}} = 0.73$. Note that $\rho_{D\bar{D}}$ is very sensitive to $\alpha_N(0)$. For example, if we set $\alpha_N(0) = -0.35$, then $\rho_{D\bar{D}} = 1.38$.

The contribution of $D\bar{D}$ exchange to the real part of the total amplitude is given by the expression

$$\rho_{D\bar{D}}=\frac{4\pi B}{\sigma_{\mathrm{tot}}^{\bar{p}p}}\int_0^{\mathrm{Im}\,f(0)}\frac{dx}{x}\,e^{-x}$$

$$\times\sin[x\rho_{D\bar{D}}\,\mathrm{Im}\,f_{D\bar{D}}(0)/\mathrm{Im}\,f(0)]. \qquad (93)$$

The results of the calculation are shown in Fig. 28 for the interval $\alpha_N(0) = -0.35$ to -0.4. It can be seen that there is good agreement with the experimental data of Refs. 87–89 and 92. The energy dependence of ρ is characteristic of the "black"-disk regime. Indeed, with decreasing energy in the region of a few giga-electron-volts the contribution of the graph in Fig. 3a is "switched on." Accordingly, the real part increases. With further decrease of the energy below 1 GeV the contribution of other annihilation mechanisms that screen $f_{D\bar{D}}$ becomes important. Therefore, ρ decreases rapidly.

The fact that we have succeeded in calculating the real part of the scattering amplitude knowing only the total cross section is one further confirmation of the importance of $D\bar{D}$ exchange in the region $p_{\mathrm{lab}} \gtrsim 1$ GeV/c. Note that this result is not a consequence of analyticity but follows merely from the chosen form of the amplitude $F(\mathbf{b})$. Dispersion relations do not give unambiguous predictions in this region (see, for example, Ref. 93).

Thus, our analysis shows that the dynamical reason for the large range of the $\bar{p}p$ interaction at low energies is unitarization of the scattering amplitude. Having described only the data on the total cross section and taken the range of the bare interaction equal to the nucleon electromagnetic radius, we have succeeded in calculating to high accuracy the elastic scattering cross section, the slope parameter, and the real part of the scattering amplitude. All this proves reliably that at low energies the partial-wave $\bar{p}p$ scattering amplitude has the form of a "black" disk.

CONCLUSIONS

In recent years, a huge amount of new experimental information has been obtained about the interaction of antiprotons from the highest to the lowest energies. In this review, we have considered the hierarchy of annihilation mechanisms associated with the decrease of the energies from the superhigh to the lowest—hundreds of mega-electron-volts. The main results of our discussion are briefly as follows.

1. In QCD perturbation theory, we have found an asymptotic annihilation mechanism associated with color-decuplet gluon exchange and formation of a three-string configuration in the final state. We have calculated the cross section of this process, $\sigma_{\{10\}} \approx (1\text{–}2) \times 10^{-27}\,\mathrm{cm}^2$, which does not depend on the energy.

2. By a statistical analysis of experimental data on the difference $\Delta\sigma_n = \sigma_n^{\bar{p}p} - \sigma_n^{pp}$ between the topological cross sections in the interval of energies 10–1500 GeV we have shown that in the region of enhanced multiplicity there does indeed exist a contribution to $\sigma_{\mathrm{ann}}^{\bar{p}p}$ that does not decrease with the energy and is equal to $(1.5 \pm 0.1) \times 10^{-27}\,\mathrm{cm}^2$.

3. The contribution of the asymptotic three-sheet annihilation mechanism to the total $\bar{p}p$ interaction cross section is apparently compensated in the region of lower values of n by the contribution of the two-sheet diagrams. The ISR data confirm this compensation.

4. In the intermediate range of energies—tens of giga-electron-volts—mechanisms associated with the presence,

in the baryon wave functions, of valence quarks with small x are dominant. In them, the spectator diquark disintegrates through color charge exchange from a color triplet state to a sextet state. The mechanisms that are associated with transfer of baryon number through a large rapidity interval (with subsequent annihilation) are part of the Pomeron, i.e., they satisfy the Eylon–Harari hypothesis. Violation of this hypothesis is due to the nonplanar correction to the ω Reggeon. This appears to be the only annihilation mechanism that contributes to the difference of the total $\bar{p}p$ and pp interaction cross sections.

5. Disintegration of a small-radius diquark requires a large transfer of transverse momentum (of order $1/r_D$). This, and also the enhanced internal momenta of the quarks in the diquark lead on its disintegration to the formation of jets with large transverse momenta. This provides a natural explanation for the fact that in annihilation events the "seagull" effect, i.e., an increasing dependence of the mean transverse momentum of the hadrons on the Feynman variable x, is strongly enhanced. In the nonannihilation channels the diquark does not disintegrate in an appreciable fraction of the events (50–60%), and the transvere momenta of the ends of the strings are determined by the reciprocal diameter of the nucleon, and not by that of the diquark.

6. With decreasing initial energy, the $\bar{p}p$ annihilation cross section increases so much that the unitarity corrections become important. Allowance for them leads to a decrease of the partial-wave amplitude of elastic scattering in the central region, this being manifested, in particular, in an appreciable growth of the interaction range. Thus, data on low-energy $\bar{p}p$ scattering have demonstrated for the first time unitarization effects analogous to those predicted earlier by the theory[65,84] for hadron interaction at superhigh energies.

7. The mechanisms responsible for annihilation at high energies also ensure transfer of baryon number through a large rapidity interval. In contrast to the widely accepted point of view, according to which a diquark is the carrier of the baryon number, baryon number can be transferred over fairly long rapidity intervals by just one valence quark (see Fig. 17) and even by gluons (see Fig. 18). Our analysis of ISR data on the difference between the cross sections for p and $\bar{p}$ production in the central rapidity region has shown that these data cannot be described in the standard form of the MQGS, but at the same time they correspond well to the prediction of the mechanism of baryon-number transfer by a single valence quark.

8. A new mechanism of baryon production has been proposed. Inclusion of decuplet exchange in the ladder diagram of the perturbative Pomeron leads to the formation of string configurations containing a pair of string junctions, on the hadronization of which a $B\bar{B}$ pair separated by a large rapidity interval is produced. In this, the mechanism differs fundamentally from the standard mode of baryon formation by production, from the vacuum, of diquark–antidiquark pairs. In this latter case, the produced baryon and antibaryon have nearly the same rapidities.

9. An important consequence of the proposed mechanism of baryon-number transfer through a large rapidity interval by means of a single valence quark is the transfer of the polarization of one of the colliding nucleons to the produced baryon. In contrast, baryon transfer through a large rapidity interval by means of a scalar diquark is obviously not accompanied by polarization transfer. In the standard form of the MQGS, polarization transfer is possible only by transfer of a vector diquark, the weight of which is evidently suppressed in the nucleon wave function. In addition, this mechanism is altogether forbidden in an important process like baryon-number transfer with production of direct Λ hyperons. Of course, it is also necessary to take into account Λ particles produced from the decay of Σ^0 and excited Σ^* hyperons, which cannot be distinguished in an experiment from direct Λ particles. Quantitative estimates made under the assumption that the three-quark states are formed in the S wave, and with allowance for the $SU(6)$ symmetry of the three-quark systems and the dominance of $\Sigma^* \Rightarrow \Lambda\pi$ decay, showed that allowance for indirect Λ hyperons does not lead to a significant change in the polarization.

10. Calculation of the probability of diquark disintegration due to transition from a color antitriplet state to a sextet state in QCD perturbation theory has shown that in the ph interactions this probability is high (40–50%). This conclusion differs fundamentally from the physical picture adopted in the standard MQGS, the Lund model, etc., in which only the fragmentation of quarks and triplet diquarks is taken into account. The possibility of describing the experimental data in these models is evidently achieved by distortion of the phenomenological diquark fragmentation functions. However, as we noted in item 8, in the case of baryon-number transfer through a large rapidity interval it is not possible to describe the data in this way.

11. For interaction of a baryon with a nucleus, multiple rescatterings increase the probability of transition of the diquark to the sextet state in comparison with scattering by a nucleon. This leads to a strong softening of the spectrum of the leading baryons. This effect is indeed observed experimentally and is usually interpreted as a consequence of the enhanced energy dissipation in the case of interaction with a nucleus (nuclear stopping power). However, from the point of view of the considered mechanism, it is not the baryon that is stopped but the baryon number. It is interesting that the same mechanism—diquark disintegration—leads to harder pion spectra; this is natural, since the energy of the quarks of the incident baryon is hardly changed in the interaction process.

In conclusion, we list briefly effects whose experimental study is most important for verification of the approach developed here.

a) Although with increasing energy the difficulties of identifying annihilation events increase, it is important to obtain data on the cross section of pp annihilation at the highest possible energies. Already at energy 100–200 GeV the relative contribution of the color decuplet exchange can become appreciable.

b) At high energies (above the ISR energy) accurate data on the difference between the topological cross sec-

tions of the $\bar{p}p$ and pp interactions are needed.

c) It would be desirable to make a comparative analysis of the momentum spectra of the pions in $\bar{p}p$ interactions in the annihilation channels and in the nonannihilation events with transfer of baryons to the central rapidity region (data on pp interactions can also be used). In addition, it would be very interesting to compare the dependences of the mean transverse momentum of the produced mesons on the Feynman variable x (seagull effect) for these two cases.

d) It is important to study experimentally the difference between the inclusive cross sections for proton and antiproton production in pp collisions in the central rapidity region at energies both above and below the ISR energies. This will make it possible to observe the appearance of the new mechanism of baryon-number transfer by means of a valence quark (at energies around 100 GeV), and also to replace this mechanism by the asymptotic mechanism associated with decuplet gluon exchange (at energies of a few tetra-electron-volts).

e) To detect the new mechanism of production of $\bar{p}p$ pairs separated by a large rapidity interval, measurements must be made of the rapidity correlations of the p and $\bar{p}$ produced in the central rapidity region in multiparticle production processes.

f) For observation of polarization transfer through a large rapidity interval, it is desirable to study the production of Λ hyperons in the central rapidity region in experiments with a polarized beam or target.

APPENDIX

Using the formula (i and j are color indices)

$$\sum_{\{10\}} \langle i_1 i_2 i_3 | \Psi_c^{\{10\}} \rangle \langle \Psi_c^{\{10\}} | j_1 j_2 j_3 \rangle = \tfrac{1}{6}[\delta_{j_1}^{i_1}\delta_{j_2}^{i_2}\delta_{j_3}^{i_3} + (\text{perm. of } j_1 j_2 j_3)],$$

we obtain from Eq. (9) the result

$$C^{\alpha_1,\ldots,\alpha_4} = \tfrac{1}{36}\langle \Psi_c^{\{1\}} | \hat{\lambda}_1^{\alpha_1}\hat{\lambda}_2^{\alpha_2}[\hat{\lambda}_1^{\alpha_3}\hat{\lambda}_2^{\alpha_4} + \hat{\lambda}_3^{\alpha_3}\hat{\lambda}_1^{\alpha_4} + \hat{\lambda}_2^{\alpha_3}\hat{\lambda}_3^{\alpha_4} - \hat{\lambda}_2^{\alpha_3}\hat{\lambda}_1^{\alpha_4} - \hat{\lambda}_1^{\alpha_3}\hat{\lambda}_3^{\alpha_4} - \hat{\lambda}_3^{\alpha_3}\hat{\lambda}_2^{\alpha_4}] | \Psi_c^{\{1\}} \rangle. \quad \text{(A1)}$$

Similarly, making the substitution $\bar{\lambda} \to \hat{\lambda}^T$ in (9), we can obtain for $\bar{C}^{\alpha_1,\ldots,\alpha_4}$ the expression

$$\bar{C}^{\alpha_1\ldots\alpha_4} = \tfrac{1}{36}\langle \Psi_c^{\{1\}} | [\hat{\lambda}_1^{\alpha_3}\hat{\lambda}_2^{\alpha_4} + \hat{\lambda}_3^{\alpha_3}\hat{\lambda}_1^{\alpha_4} + \hat{\lambda}_2^{\alpha_3}\hat{\lambda}_3^{\alpha_4} - \hat{\lambda}_2^{\alpha_3}\hat{\lambda}_1^{\alpha_4} - \hat{\lambda}_1^{\alpha_3}\hat{\lambda}_3^{\alpha_4} - \hat{\lambda}_3^{\alpha_3}\hat{\lambda}_2^{\alpha_4}]\hat{\lambda}_1^{\alpha_1}\hat{\lambda}_2^{\alpha_2} | \Psi_c^{\{1\}} \rangle. \quad \text{(A2)}$$

When the expressions (A1) and (A2) are substituted in (12), we obtain 36 terms, of which the following seven terms are independent:

$$C_1 = (1212)(2121); \quad C_2 = (1212)(1221);$$

$$C_3 = (1231)(1321);$$

$$C_4 = (1231)(3112); \quad C_5 = (1231)(3121);$$

$$C_6 = (1212)(1321), \quad C_7 = (1212)(2321).$$

where we have used the abbreviation

$$(i_1 i_2 i_3 i_4)(j_1 j_2 j_3 j_4) \equiv \frac{1}{6^4} \sum_{\alpha_1\ldots\alpha_4=1}^{8} \langle \Psi_c^{\{1\}} | \hat{\lambda}_{i_1}^{\alpha_1}\hat{\lambda}_{i_2}^{\alpha_2}\hat{\lambda}_{i_3}^{\alpha_3}\hat{\lambda}_{i_4}^{\alpha_4} | \Psi_c^{\{1\}} \rangle \times \langle \Psi_c^{\{1\}} | \hat{\lambda}_{j_1}^{\alpha_4}\hat{\lambda}_{j_2}^{\alpha_2}\lambda_{j_3}^{\alpha_3}\lambda_{j_4}^{\alpha_4} | \Psi_c^{\{1\}} \rangle.$$

The factor C (12) can be expressed in terms of C_{1-7} as follows:

$$C = 2C_1 - 2C_2 + 4C_3 + 4C_4 - 8C_5 + 8C_6 - 8C_7. \quad \text{(A3)}$$

The factors C_1–C_7 were calculated using the Fierz identity

$$\sum_{\alpha=1}^{8} (\hat{\lambda}^\alpha)_k^i (\hat{\lambda}^\alpha)_m^n = -\tfrac{2}{3}\delta_k^i\delta_m^n + 2\delta_m^i\delta_k^n,$$

which makes it possible to carry out the summation over $\alpha_1,\ldots,\alpha_4$ in the expressions for C_1–C_7. The summation over the quark color indices can be made using the color wave function

$$\langle i_1 i_2 i_3 | \Psi_c^{\{1\}} \rangle = \frac{1}{\sqrt{6}} \varepsilon_{i_1 i_2 i_3}.$$

Substitution of the values of the factors C_1–C_7, obtained as a result of laborious calculations, in (A3) gives the value used in the text: $C = 160/9$.

[1)] We assume that the baryons consist of three valence quarks, i.e., that they do not contain sextet diquarks. This is confirmed by the experimental fulfillment of s-channel factorization relations,[18] which use this picture.

[2)] Note that this energy dependence of the annihilation cross section is in no way related to the contribution of the planar Reggeons to the difference between the total cross sections of the $\bar{B}B$ and BB processes. This last contribution is absent, for example, in the $\bar{\Delta}^- \Delta^{++}$ interaction cross section (because of the exotic quantum numbers in the s channel), while the annihilation cross section depends on the energy as $s^{-1/2}$.

[3)] In principle, the energy dependence of the contribution to $\alpha_{\text{ann}}^{\bar{B}B}$ from the mechanisms of Figs. 6a and 7 can be influenced by the tunneling production of constituent gluons in the chromoelectric field of the decuplet and sextet tubes, since their production can lead to nonannihilation channels. However, estimates based on Schwinger's formula for the probability of particle production in a constant field show that the part played by these processes is negligibly small, owing to the large mass of the constituent gluon ($M_g \approx 0.7$ GeV/c^2; Ref. 47).

[4)] Although a sextet string is energetically more advantageous than two triplet strings,[46] the latter can decay independently, since they form a V-shaped configuration in space because of the large internal Fermi momentum of the quarks in the diquark.

[5)] In Ref. 38, α_s was normalized on the basis of the condition $\sigma(NN \to N_{\{8\}}N_{\{8\}}) = \sigma_{\text{tot}}^{NN}$. Because the intermediate states for the cutting of the two-gluon exchange diagram do not contain elastic and diffraction channels, it appears more reasonable to use σ_{in}^{NN}, and not σ_{tot}^{NN}, to normalize α_s in this procedure. Then $\sigma_{\{10\}}$ is reduced by a factor ~ 1.5.

[6)] In Ref. 56, a procedure was proposed for determining $\sigma_{\text{ann}}^{\bar{p}p}$ from the inclusive cross sections for $\bar{p}p$ annihilation. Analysis of data at $p_{\text{lab}} = 32$ GeV/c (Ref. 57) showed that the dependence observed at $p_{\text{lab}} \sim 10$ GeV/c, $\sigma_{\text{ann}}^{\bar{p}p} \propto s^{-1/2}$, is also maintained at these energies. However, even with this information, separation of a constant contribution of about 10^{-27} cm^2 is impossible because of the large $\bar{p}p$ annihilation cross section and large experimental errors.

[7)] It is possible that it is the neglect of this additional screening that makes it necessary to introduce large values of the coefficients of the shower enhancement of $\omega\mathbb{P}$ branchings to describe the crossover effect in pp and $\bar{p}p$ scattering in the quasi-eikonal model.[63]

[1] G. Cohen-Tannoudji, A. E. Hassouni, J. Kalinowski, and R. Pesehanski, Phys. Rev. D **19**, 3397 (1979).
[2] A. B. Kaĭdalov, Pis'ma Zh. Eksp. Teor. Fiz. **32**, 494 (1980) [JETP Lett. **32**, 474 (1980)].
[3] A. B. Kaĭdalov, Phys. Lett. **116B**, 459 (1982).
[4] A. B. Kaĭdalov, *Elementary Particles. Tenth School of Physics of the Institute of Theoretical and Experimental Physics*, No. 2 [in Russian] (Énergoatomizdat, Moscow, 1983), p. 3.
[5] A. Capella and J. Tran Thanh Van, Phys. Lett. **114B**, 450 (1982).
[6] A. B. Kaĭdalov and K. A. Ter-Martirosyan, Yad. Fiz. **39**, 1545 (1984) [Sov. J. Nucl. Phys. **39**, 979 (1984)].
[7] A. B. Kaĭdalov and K. A. Ter-Martirosyan, Yad. Fiz. **40**, 211 (1984) [Sov. J. Nucl. Phys. **40**, 135 (1984)].
[8] A. I. Veselov, O. I. Piskunova, and K. A. Ter-Martirosyan, Phys. Lett. **158B**, 175 (1985).
[9] G. Veneziano, Phys. Lett. **52B**, 220 (1974); Nucl. Phys. **B74**, 365 (1974).
[10] G. F. Chew and C. Rosenzweig, Phys. Rep. **41**, 264 (1978).
[11] F. E. Low, Phys. Rev. D **12**, 163 (1975).
[12] A. Casher, H. Neuberger, and S. Nussinov, Phys. Rev. D **20**, 179 (1979).
[13] E. G. Gurvich, Phys. Lett. **87B**, 386 (1979).

Translated by Julian B. Barbour